The Pennsylvania State University
APPLIED RESEARCH LABORATORY
Post Office Box 30
State College, PA 16804

Numerical Predictions for the Demo Enclosure Comparison to Experiment

by

J. B. Fahnline, R. L. Campbell, and S. A. Hambric

Technical Report 04-007
May 2004

E. G. Liszka, Director
Applied Research Laboratory

REPORT DOCUMENTATION PAGE

Form Approved OMB No. 0704-0188

1. REPORT DATE *(DD-MM-YYYY)*	2. REPORT TYPE	3. DATES COVERED *(From - To)*
May 2004	Technical Report	

4. TITLE AND SUBTITLE

Numerical Predictions for the Demo Enclosure and Comparison to Experiment

5a. CONTRACT NUMBER
PL01000100

5b. GRANT NUMBER

5c. PROGRAM ELEMENT NUMBER

6. AUTHOR(S)

J. B. Fahnline, R. L. Campbell, and S. A. Hambric

5d. PROJECT NUMBER

5e. TASK NUMBER

5f. WORK UNIT NUMBER

7. PERFORMING ORGANIZATION NAME(S) AND ADDRESS(ES)

Applied Research Laboratory
Post Office Box 30
State College, PA 16804

8. PERFORMING ORGANIZATION REPORT NUMBER

TR 04-007

9. SPONSORING / MONITORING AGENCY NAME(S) AND ADDRESS(ES)

10. SPONSOR/MONITOR'S ACRONYM(S)

11. SPONSOR/MONITOR'S REPORT NUMBER(S)

12. DISTRIBUTION / AVAILABILITY STATEMENT

Approved for public release, Distribution unlimited

13. SUPPLEMENTARY NOTES

14. ABSTRACT

Numerical methods for modeling the surface vibrations and sound radiation from a small enclosure are investigated, with special emphasis on simple methods for representing the connections. Finite element methods are used for the structural vibrations and the accompanying sound radiation is computed using the boundary element method. It is shown that good results can be obtained by simply adjusting the resonance frequencies for the modes to agree with experimental measurements. This assumes that the modes are fairly similar and that a one-to-one correspondence can be established between the numerical and experimental results. It is also shown that the technique of analyzing the components separately and combining them together using adding stiffnesses performed as well or better than trying to model the connections directly. The technique is also well-suited to optimization problems because numerous cases can be analyzed much more quickly than the more direct technique. Comparisons to experimental measurements show that the strategies for combining the components worked better for the more rigid connections than they did for the softer configurations.

15. SUBJECT TERMS

16. SECURITY CLASSIFICATION OF:			17. LIMITATION OF ABSTRACT	18. NUMBER OF PAGES	19a. NAME OF RESPONSIBLE PERSON
a. REPORT	b. ABSTRACT	c. THIS PAGE			19b. TELEPHONE NUMBER *(include area code)*
UNCLASSIFIED	UNCLASSIFIED	UNCLASSIFIED	Unclassified Unlimited-UU	49	

Standard Form 298 (Rev. 8-98)
Prescribed by ANSI Std. Z39.18

TABLE OF CONTENTS

Page Number

LIST OF TABLES

LIST OF FIGURES

LIST OF FIGURES (CONT'D)

LIST OF FIGURES (CONT'D)

INTRODUCTION

The "demo enclosure" is a small box meant to simulate the basic characteristics of an equipment enclosure, but without the complexity of an actual enclosure. Extensive experimental measurements have been made on the enclosure and are summarized in a companion report entitled "Experimental Measurements of the Demo Enclosure". In this report, we will summarize the associated numerical modeling of the enclosure's structural vibration and radiated sound field using finite and boundary element techniques.

One of the main goals of the report is to establish useful modeling guidelines for finite and boundary element analyses of enclosures. Producing accurate predictions is of primary importance, but ease of implementation is also important. We will try to demonstrate that it is not always beneficial to try to duplicate all the enclosure's structural complexity in the finite and boundary element models because errors inevitably occur and it is frequently difficult to adjust the models without considerable effort. For example, it is relatively simple to produce accurate models for shelves and enclosures separately, but their interconnections are much more difficult to represent. When the models are combined into much larger finite element models, it becomes difficult and time consuming to optimize the modeling of the interconnections. Our research was thus directed towards developing simple methods for adjusting the individual models and combining them together after an initial finite element analysis.

A. Finite Element Modeling

Before beginning the analysis, we will first discuss the basic procedures used to create the finite and boundary element models. To construct a finite element model, a geometric representation of the structure is created and then meshed. The user has considerable latitude in dividing the structure into geometrical entities and meshing them. On one extreme, the structural geometry can be represented in terms of a few compound shapes, and then "automeshed" within a finite element pre-processor. On the other extreme, the geometry can be broken down into many small pieces and meshed individually using "mapped meshes". While it is certainly easier to generate meshes using automeshing, it is difficult to produce a mesh with uniform density. As an example, the left side of Figure 1 shows a portion of the demo enclosure that is represented as a single geometric entity. The white dots along the edges are mesh seeds specified by the user to control the mesh density. Performing the automesh command then yields the tetrahedral (linear 4-noded) solid mesh of the enclosure shown on the right side of the figure. Although the mesh is reasonable, the elements along the edges and near the corners are more refined and not uniformly spaced. Automeshing procedures thus lead to larger models and increased computational expense, but are relatively easy to generate. This is especially true as the mesh resolution increases and more elements are required along the edges. To demonstrate, Table 1 lists the first six resonance frequencies for a series of linear tetrahedral meshes with different densities created using automeshing procedures. The results show that the predictions for the resonance frequencies converge very slowly as a function of mesh density.

Better convergence and more uniform meshes can be obtained by dividing the geometry into smaller pieces and meshing them individually. The left side of Figure 2 shows the same geometry when it is divided up into smaller pieces and the right side shows the resulting mesh.

Even though the full finite element model now only has 77,390 nodes and 18948 elements, it yields predictions of 55.86, 61.52, 74.19, 76.04, 80.59, and 82.90 Hz for the first six resonance frequencies, which are far more accurate than those of even the finest tetrahedral mesh (as compared to predictions of 55.41, 61.17, 73.72, 75.45, 80.35, and 82.38 from a more refined "uniform" mesh with 172,210 nodes and 43,008 elements). This example might seem somewhat misleading because both shell and hexahedral elements were used in creating the mapped meshes, considerably reducing the total degrees of freedom. However, it would be impossible to combine these two element types together without breaking the geometry down into smaller pieces before it is meshed, thus excluding automeshing.

B. Boundary Element Modeling

Once the finite element analysis has been performed, the fluid-coupling and radiated acoustic field can be predicted using the boundary element method. The first step in the process is to generate an acoustic element mesh corresponding to the finite element mesh. The nodes for the acoustic mesh must match those in the finite element model so that the mode shapes from the structural analysis can be input to the acoustic analysis. The acoustic mesh represents only the boundary surface of the structure in contact with the fluid.

In general, a boundary element model of an enclosure would include both internal and external surfaces because both are contact with air. However, it would be difficult to generate a boundary element model of the interior acoustic field with correct representations for the shelf and the electrical components and the extra acoustic elements can increase the computation times considerably. Thus, it is desirable to simplify the boundary element analysis and only include the exterior acoustic field or a simplified representation of the interior. This is also beneficial because it would be very time consuming to generate separate boundary element models for every electrical equipment configuration. As an example of a simplified model of the interior, we might eliminate the middle and bottom shelf from the analysis and just assume the fluid is free to flow anywhere inside the enclosure, as illustrated in Figure 3. This decreases the number of acoustic elements in the model by approximately 40 %. In theory, this will reduce the analysis time by 78 % because the time required to perform the matrix inversions is proportional to the number of elements cubed.

As an initial step to try to verify the simplified acoustic model, we will demonstrate that the surface vibrations are relatively insensitive to whether or not the internal acoustic field is represented in the model. Intuitively, we expect this to be true since mode shapes and resonance frequencies typically do not shift significantly due to fluid-coupling for in-air applications because the overall stiffness and mass of the air is small in comparison to the structural stiffness and mass. We will perform the test on the configuration without the interior shelf since its inclusion will generally increase the overall structural stiffness of the enclosure. Figure 4 shows the integrated squared normal velocity over the enclosure walls for a drive point located near a corner of one of the sides both with and without the interior acoustic field included in the analysis. The main differences occur between 75 and 100 Hz, where the fundamental interior acoustic resonance is located. Similar results are shown in Figure 5 for the acoustic power output. Even though the interior acoustic field only effects the surface vibrations near the fundamental acoustic resonance, we will include it in the subsequent analyses, but without the interaction with the middle and bottom shelves.

C. Shelf Alone

Our basic strategy for modeling the full enclosure will be to first generate models of the shelf and enclosure separately, validate them, and then combine them together to create the full model. We will begin with the shelf alone, the finite element model for which is shown in Figure 6. The model is composed of three sets of elements, one modeling the thin plating (grey in the figure), one modeling the angle brackets (light blue), and an overlapping set of elements enforcing continuity of rotations between the plating and angle brackets (gold). To properly account for the structural mass, the overlapping elements have the same Young's modulus as the plate, but negligible mass. All of the pieces are made of aluminum, and the dimensions are given in the companion report.

To validate the model, we will compare the finite element predictions to the experimental measurements of the shelf sitting on "bubble-wrap". Figure 7 shows a comparison of the first four modes from the experimental measurements and numerical predictions. Clearly, the mode shapes are well represented in the finite element model, but the resonance frequencies are somewhat too high, indicating the finite element model is too stiff. Similarly, Figure 8 shows a comparison of the integrated normal velocity over the surface of the plate for the original finite element model and the experimental data, which also indicates that the model is too stiff. The explanation for the discrepancy is fairly simple. In the model, each set of nodes at the interface between the shelf and the brackets has been coalesced, whereas, in reality, the angle brackets are not welded to each other and are only connected to the shelf plating at approximately two-inch intervals.

Rather than trying to modify the finite element model to make it more closely correspond to the experimental data, we can manually adjust the resonance frequencies and damping loss factors to make them match better. This is possible because the modal stiffness and damping only enter the analysis through the resonance frequencies and damping loss factors, which can be adjusted manually after the initial finite element computations. The analysis assumes a one-to-one match between the numerical and experimental mode shapes. After adjusting the modal frequencies and loss factors, the numerical predictions and experimental measurements agree very closely, as shown in Figure 9. The remaining relatively small differences are presumably due to the rigid body modes of the shelf, which occur at nearly zero frequency in the numerical model. While the results are excellent for this simple example, the process will obviously become more difficult for more complicated structures and finite element models. Nonetheless, we will demonstrate it can yield excellent results for models of the size of the demonstration enclosure.

D. Enclosure without the Shelf

The second step is to construct a finite element model of the enclosure without the shelf. Mapped meshing algorithms were used to construct the finite element models even though the process is somewhat tedious and time consuming. However, once the geometry has been created, it is relatively simple to refine the mesh by changing the mesh seeds along the edges, making it possible to perform convergence tests. Figure 10 shows a comparison of the integrated squared normal velocity for two mesh densities for a drive point on one of the sides. The results are nearly identical up to 500 Hz except for a slight downward shift in the resonance frequencies for the more

refined mesh. Thus, because the results are nearly identical, we will use the less refined mesh for the subsequent analyses.

Once the structural model has been validated, a second convergence check is performed for the acoustic radiation predictions. Figure 11 shows the two acoustic meshes used in the analysis with 832 and 1980 elements. In the figure, each color represents a different acoustic element. Recalling that the computation times for the acoustic calculations are approximately proportional to the number of acoustic elements cubed, we expect the finer mesh to require 13.5 times longer per frequency. In actuality, the computation times for the denser acoustic mesh are only 3.2 times longer, indicating that, while the matrix inverse accounts far a large part of the time, other calculations are also significant contributors. This is especially true for the coarser acoustic model, because the time required for the matrix inverse is much smaller. Convergence analyses were performed both with and without internal acoustic fields, and Figure 12 shows a comparison of the radiated acoustic power output for the case with the internal field included. Since the predictions agree very closely, we will use the coarser acoustic mesh with 832 elements in the subsequent analyses.

To further validate the model, we will compare the predictions to measured mode shapes and transfer function data. Figure 13 shows a comparison of the first four experimental and numerical mode shapes and resonance frequencies for the configuration without the shelf. As for the shelf alone, the finite element models are somewhat too stiff, presumably due to the 2-inch spacing for the screws in the actual enclosure. Figure 14 shows a comparison of the integrated squared normal velocity for the experimental measurements and numerical predictions. The drive point location and direction are illustrated in the overlaid picture of the finite element mesh.

We can again alter the finite element model to make it correspond more closely to the experimental measurements by manually adjusting the resonance frequencies and damping loss factors. For a model of this complexity, a MAC (modal assurance criteria) analysis is very useful in helping to identify a one-to-one correspondence between the experimental and numerical mode shapes. Figure 15 lists sample output for the MAC for the enclosure without the shelf. The first column of numbers lists the experimental modes and the last eight columns list the four closest matching numerical modes and their associated MAC levels. The first six experimental modes are essentially rigid body and are not duplicated in the numerical model. In general, MAC levels above 0.8 are desirable, but even levels in the range of 0.5 can indicate a close match if the accelerometer density is somewhat coarse and the levels for the secondary modes are low. Figure 16 shows the revised comparison for the integrated squared normal velocity after the resonance frequencies and loss factors are adjusted in the numerical model. The correspondence is excellent below 300 Hz and is acceptable between 300 and 400 Hz. The main discrepancy in the lower frequency range occurs near the fundamental internal acoustic resonance at approximately 75 Hz, which is either very heavily damped or missing in the experimental data.

Although no pressure data was taken for the enclosure without the shelf, we can still obtain some level of validation by comparing the fully numerical predictions to those using the measured vibration data as input to the acoustic boundary element program. Figure 17 shows the predicted acoustic power output as a function of frequency for the two cases. The two predictions agree reasonably well, although the power output predictions using the experimental surface vibrations as

input are consistently high, especially in the higher frequency range. This is expected because the experimental measurement grid is too coarse to properly resolve the phase variations across the acoustic elements. Destructive interference effects are then lost and the power output predictions are consistently too high. Our basic conclusion from the individual component analysis is that the finite element models are somewhat too stiff, but that their resonance frequencies and damping loss factors can be adjusted to yield excellent comparisons to the experimental measurements.

E. Enclosure with the Shelf Resting on Sorbothane

Of the configurations tested experimentally, the shelf resting on sorbothane (simulating an isolation mount) is the most difficult to model using finite elements. Even with good specifications for the material properties and dimensions, the sorbothane is difficult to model because it is not tied to the shelf or the enclosure except through gravity, the effects of which are typically neglected in our finite element models. The actual connection properties could conceivably be determined experimentally and represented in the finite element model using bar or beam elements, but it would be expensive and time consuming to design and build the required special purpose apparatus. Rather than trying to modify our standard procedure, we will simply try to model the material properties and dimensions as well as possible in a model combining the shelf and the enclosure. The other possibility is to generate separate models of the components, and then combine them to create a complete model. This speeds up the analysis considerably, and allows the connection properties to be optimized. We will apply both methods to the problem to determine which yields the most accurate and efficient numerical solution.

To start, we will try to combine the two components into a larger finite element model, with correct representations for the sorbothane's dimensions and material properties. Figure 18 shows one quarter of the resulting finite element model along with a close-up of the sorbothane connection, which is shown as dark blue. Two 20-node brick elements through the thickness are used to represent the sorbothane, which should be more than sufficient to correctly model the stresses and strains. No other connections between the shelf and the enclosure exist in the model. Figure 19 shows a comparison of the experimental measurements and numerical predictions of the integrated squared normal velocity over the enclosure walls for a drive point on the shelf. Obviously, the representation of the sorbothane in the finite element model is much too soft because very little energy is transferred from the shelf to the enclosure. Figure 20 shows a similar comparison after the resonance frequencies and loss factors were manually adjusted to make them match the measurements. Although the resonance frequencies now line up better, the connection is still much too soft and the vibrations of the enclosure are much too low.

The alternative is to connect the shelf to the enclosure through stiffnesses and then adjust their magnitude to correctly represent the level of coupling. As a first step, the shelf and enclosure finite element models were combined together and the structural analysis was rerun. This helps to ensure that none of the element and node numbers overlap for the two models. The resonance frequencies should be identical to those for the separate models. To connect the components, four sets of nodes at the corners of the shelf and inside of enclosure are connected with stiffnesses. The analyst simply specifies the four sets of nodes along with the stiffness in each direction. Figure 21 shows a comparison of the experimental measurements and numerical predictions of the integrated squared normal velocity over the enclosure walls for a drive point on the shelf. Several different

stiffnesses were tested to try to find the best match to the experimental measurements. Although there are still some differences in the vibration spectra, a value of Kz=1x10^6 gives a reasonably good match to the measurements. Using the optimized stiffnesses, Figure 22 shows a comparison of the experimental measurements and numerical predictions of the acoustic power output for a drive point on the shelf. We recall from the previous report summarizing the experimental measurements that two sets of tests were performed; one to measure the surface vibrations and one to measure the radiated pressures. For the pressure measurements, two shakers were added to the shelf, resulting in downward shifts in the resonance frequencies for some of the modes. Thus, some of the discrepancies in the power output comparison, and specifically the mode at approximately 140 Hz, are due to the addition of the shakers rather than the fidelity of the finite or boundary element models. The results show that the power output predictions are much more accurate when the two models are connected with discrete stiffnesses. However, in a more general situation, it is unlikely that the desired vibration spectrum will be specified in advance, so that the process of optimizing the connection stiffnesses becomes much more difficult. Nonetheless, the analysis is useful because numerous configurations can be tested very efficiently.

F. Enclosure with the Shelf Hinged to the Enclosure

For the second configuration, the shelf is attached to the enclosure using hinges. We will again model the connections directly using added stiffnesses. When the connections are modeled directly, an extra row of hexahedral elements is added around the periphery of the plate and one of the outer rows of nodes is tied to the enclosure plating. Because the hexahedral elements only have displacement degrees of freedom, the shelf and plate are free to rotate independently, simulating a hinged connection. Figure 23 shows a comparison of the experimental measurements and numerical predictions of the integrated squared normal velocity over the enclosure walls for a drive point on the shelf. Because both the models of the shelf and the enclosure are too stiff, it is not surprising that the combined model is also too stiff. Figure 24 shows a similar comparison when the resonance frequencies and damping loss factors are adjusted for the combined finite element model. Although the comparison improves, the vibration levels for the numerical model are still too low, presumably because our technique does not allow the admittance levels to be adjusted.

When the connections are modeled using added stiffnesses, the main difficulties are in identifying the relevant nodes and directions and optimizing their values. For the hinged connection, stiffnesses were added in all three directions at approximately two-inch spacing around the periphery of the shelf. The values along the hinge were taken to be different than that in the plane in which it rotates. To help in generating the connections, layers were used in FEMAP (a finite element pre-processor) to isolate only the components of interest, making the process far less susceptible to user error. Seventeen test cases were run to identify the optimum values for the stiffnesses. Despite testing many configurations with different values in the two directions, specifying the same value for the stiffness in all three directions yields the best results. For the optimized configuration, Figure 25 shows the comparison between the experimental measurements and numerical predictions of the integrated squared normal velocity over the enclosure walls for a drive point on the shelf. Overall, the two sets of predictions compare reasonably well, with the major differences occurring in the frequency range between 130 and 150 Hz. The missing peaks are actually present in the combined model, but are not excited to nearly the same level. The screws used to connect the shelf to the walls are steel and have 1/4" diameter, and thus we would

expect their stiffness to be approximately equal to A E / L = 6.3 x 10^6 Newtons / L. The value for L depends on the spacing between the head of the screw and the nut, and will be a small fraction of a meter. Thus, the optimized value for the stiffnesses is somewhat lower than that of the screws.

For the power output predictions, the acoustic model includes both interior and exterior acoustic fields, but does not include the effects of the shelf. Figures 26-28 show comparisons of the radiated acoustic power level between the experimental measurements and the numerical predictions for the various prediction strategies. As for the previous configurations, the differences between the predictions and the measurements are largely due to differences in the vibration profiles rather than the boundary element computations. The main challenge is thus to correctly model the structural vibrations in the finite element analysis.

G. Enclosure with the Shelf Clamped to the Enclosure

In the final configuration, the shelf is clamped to the enclosure walls. For the combined model with direct connections, the previous model used for the hinged configuration was modified so that two rows of nodes are tied to the enclosure plating rather than just one. This allows moments to be transferred between the components. Figures 29 and 30 show comparisons of experimental measurements and numerical predictions of the integrated squared normal velocity over the enclosure walls for a drive point on the shelf before and after the frequencies and loss factors are adjusted. In this case, the comparison is relatively good even without adjusting the frequencies and it is very good after they are adjusted. As for the hinged plate, the vibration levels for the numerical model are somewhat low, presumably because our technique does not allow the admittance levels to be adjusted.

When the connections are modeled using added stiffnesses, two sets of nodes were tied together with stiffness to simulate the locations of the screws. In this case, the stiffnesses in the three directions were taken to be equivalent and eight configurations were tested to determine the optimum values. For the optimized configuration, Figure 31 shows the comparison between the experimental measurements and numerical predictions of the integrated squared normal velocity over the enclosure walls for a drive point on the shelf. Overall, the two sets of predictions compare very well, with major differences only beginning to occur above 300 Hz.

For the power output predictions, the acoustic model again includes both interior and exterior acoustic fields, but does not include the effects of the shelf. Figures 32-34 show comparisons of the radiated acoustic power level between the experimental measurements and the numerical predictions for the various prediction strategies. The agreement is excellent when the connections are modeled with added stiffnesses. As for the previous configurations, the differences between the predictions and the measurements are largely due to differences in the vibration profiles rather than the boundary element computations.

CONCLUSIONS

Several conclusions can be drawn from our numerical modeling of the demonstration enclosure. First and foremost, the strategies for combining the components worked better for the more rigid connections than they did for the softer configurations. This may be a potential

weakness in the future because it is desirable to isolate the shelves as much as possible from the enclosure to reduce sound radiation. Our second conclusion is that the simple method of adjusting the frequencies and damping loss factors in the numerical models can be very effective, provided the requisite experimental data is available. Minor discrepancies occur in the predictions because the admittance levels are not adjusted, but the differences are relatively small for the problems examined. Third, the technique of analyzing the components separately and combining them together using adding stiffnesses performed as well or better than trying to model the connections directly. The technique is also well-suited to optimization problems because numerous cases can be analyzed much more quickly than the more direct technique. However, because experimental measurements were used to tune the values for the stiffnesses, it is doubtful that the predictions would be nearly as accurate without the tuning process. Finally, the differences between the predictions and the measurements are largely due to differences in the finite element predictions of the vibration profiles rather than the boundary element computations. The main challenge is thus to correctly model the structural vibrations in the finite element analysis.

FUTURE WORK

The demo enclosure has provided us with useful general recommendations, but it has not given us much opportunity to test specific practical configurations. This is especially important because the results have shown that it is beneficial to mount the shelves as softly as possible, but the previous practical enclosure designs have used welded connections exclusively. Methods for experimentally testing the connections and modeling them in the finite element analyses would also be very helpful.

Table 1. The first six resonance frequencies for the enclosure without the shelf using automatic meshing

	Mesh 1	Mesh 2	Mesh 3	Mesh 4	Mesh 5
# Nodes	224334	152645	317937	424245	606810
# Elements	11240	76327	158919	212177	303432
F1	80.58	60.08	58.52	58.38	58.18
F2	89.53	65.42	63.68	63.52	63.30
F3	93.98	78.86	77.24	76.73	76.48
F4	143.18	83.73	81.86	81.46	81.13
F5	157.27	84.43	82.42	81.62	81.35
F6	160.92	85.91	82.98	82.50	82.30

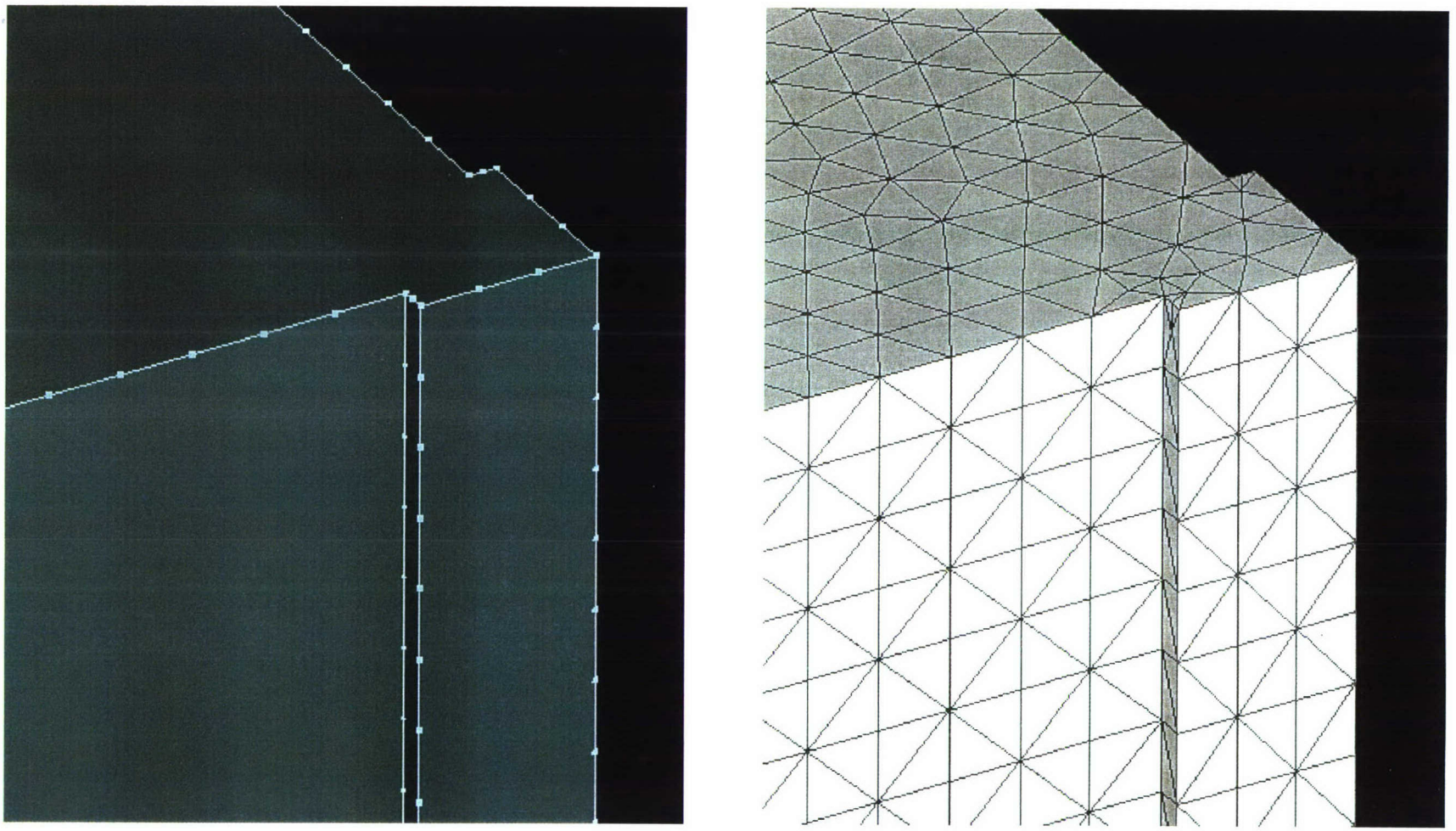

Figure 1. Mesh seeds and resulting finite element mesh using automatic meshing

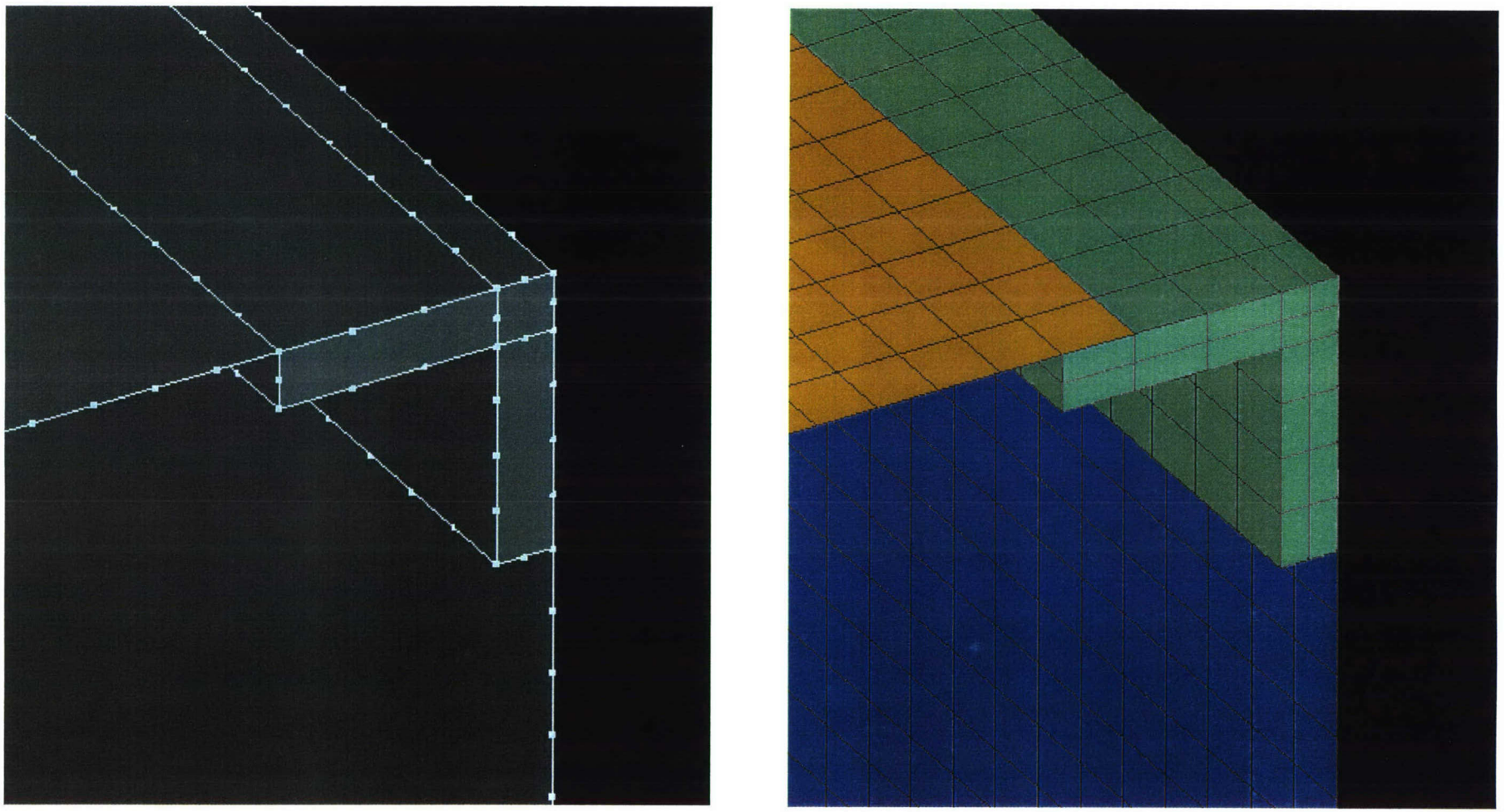

Figure 2. Mesh seeds and resulting finite element mesh using mapped meshing

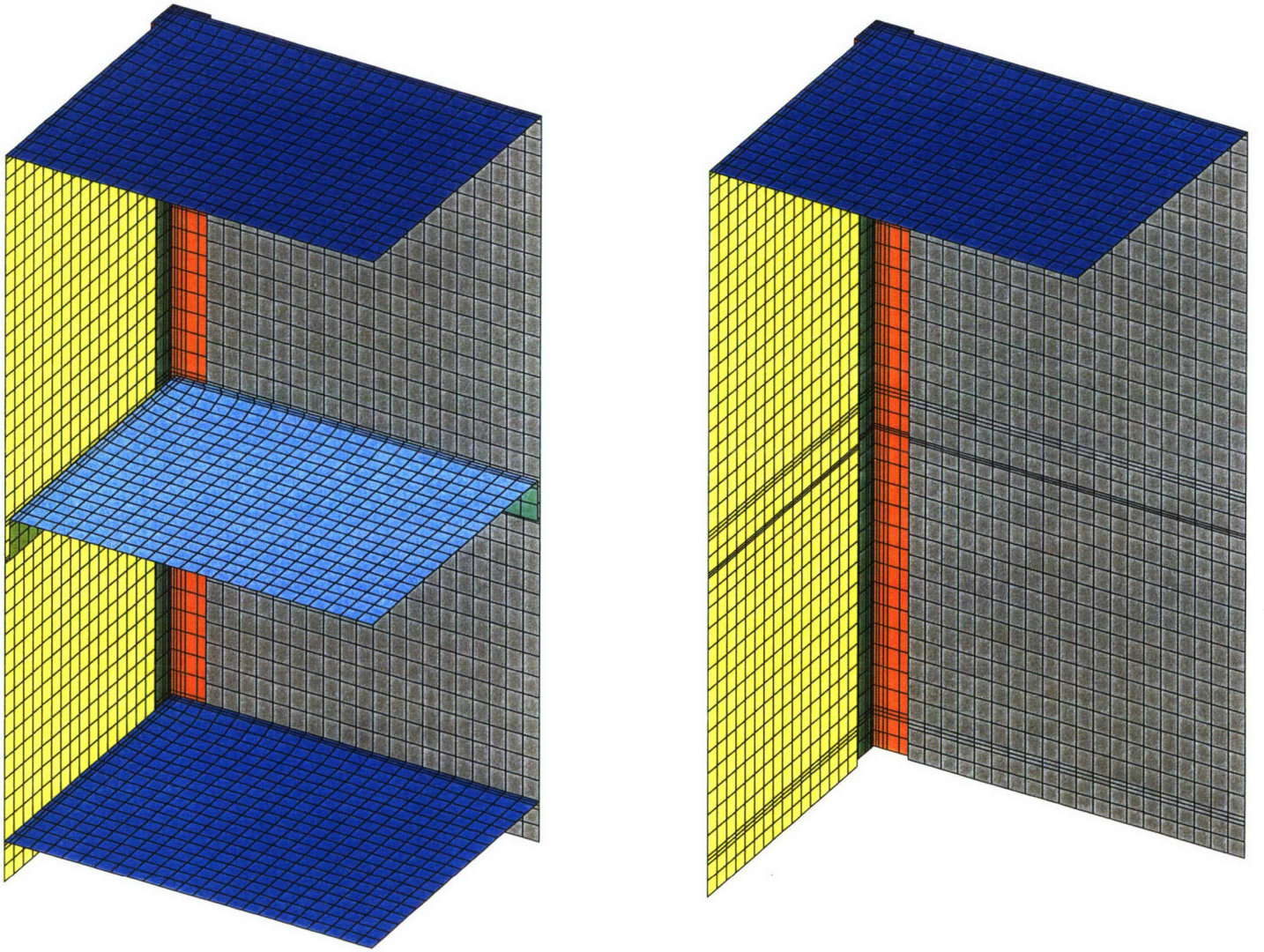

Figure 3. Boundary element models with and without the interior and bottom shelves

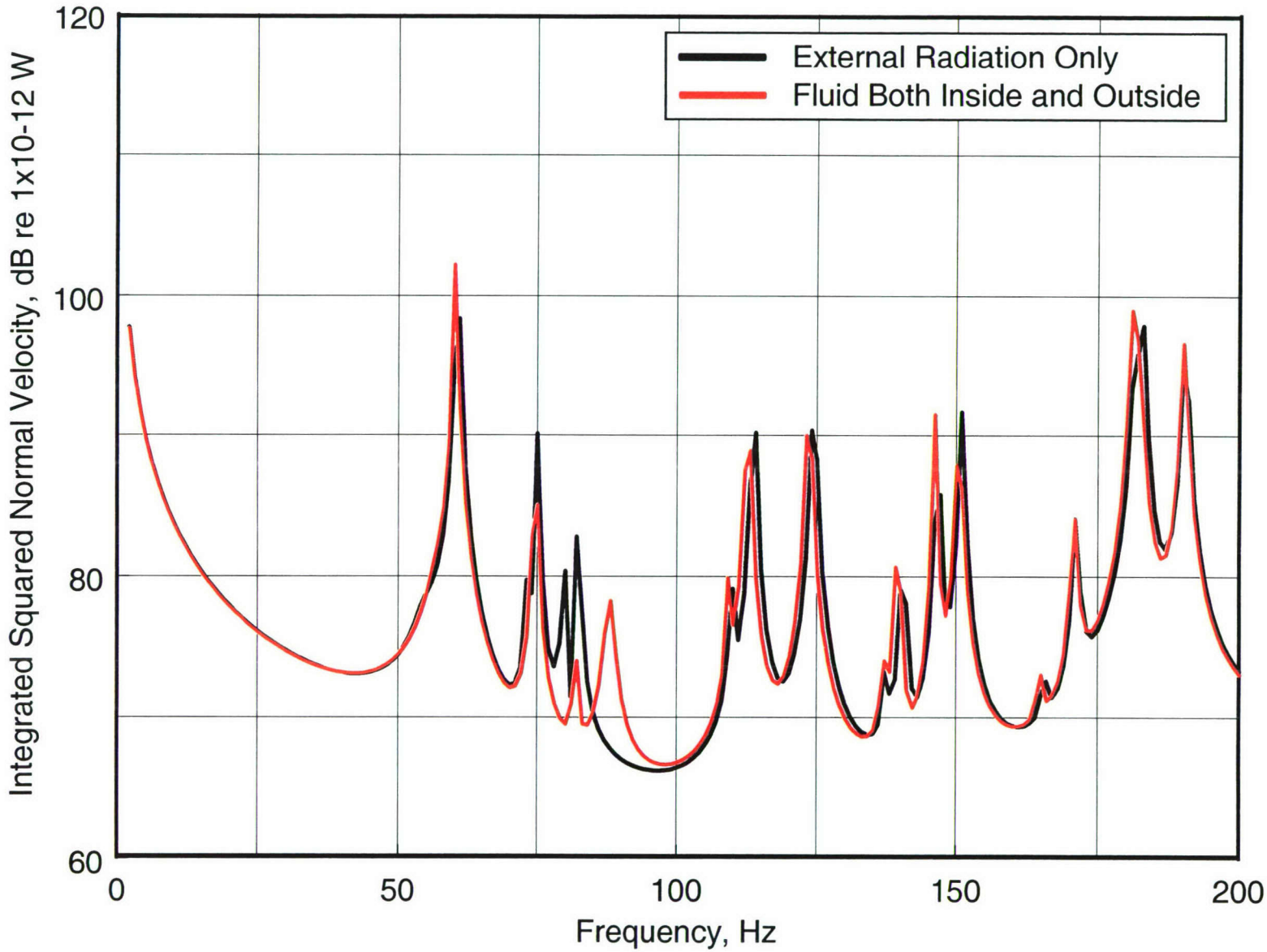

Figure 4. Integrated squared normal velocity for the two different boundary element models

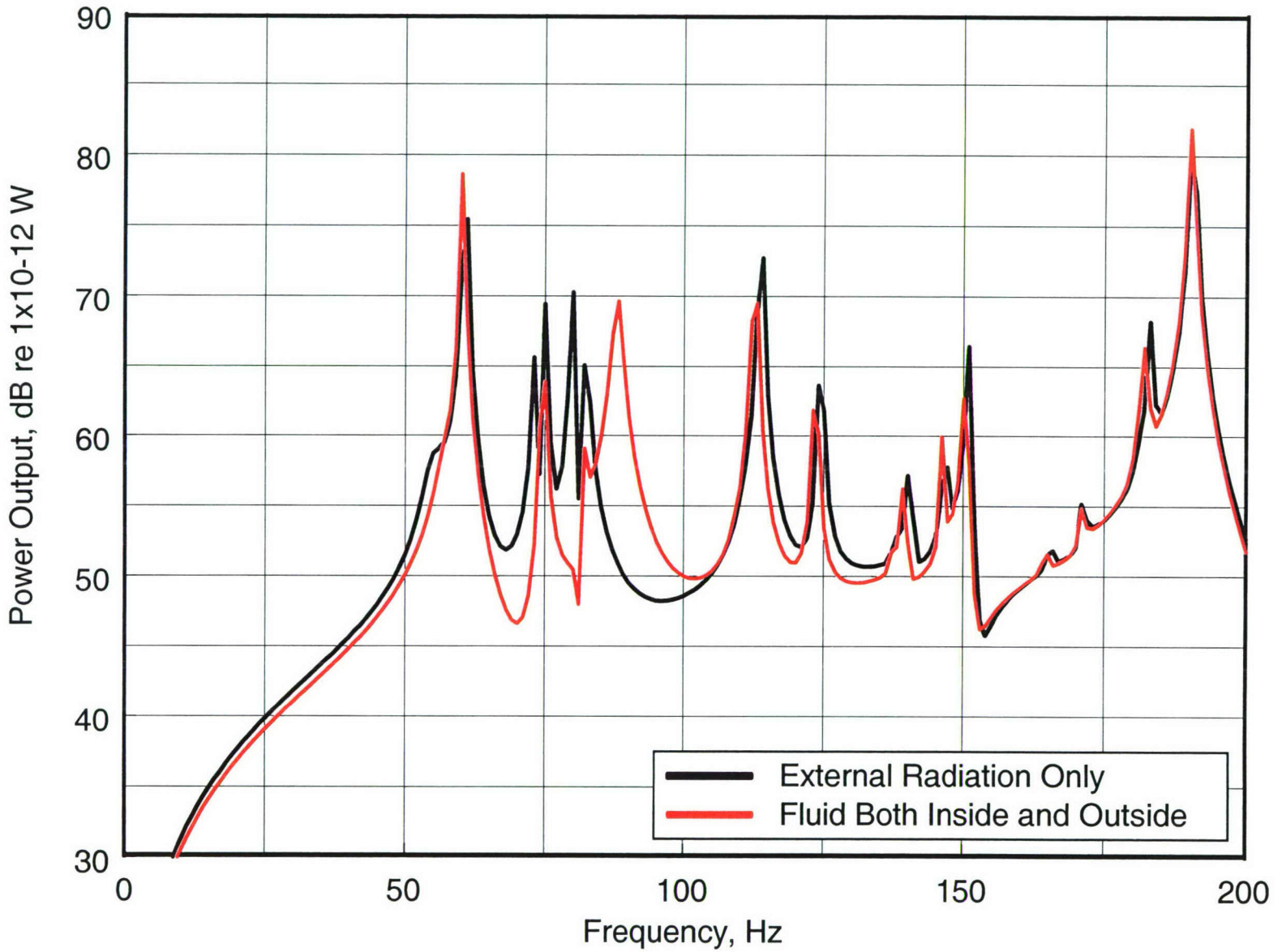

Figure 5. Acoustic power output for the two different boundary element models

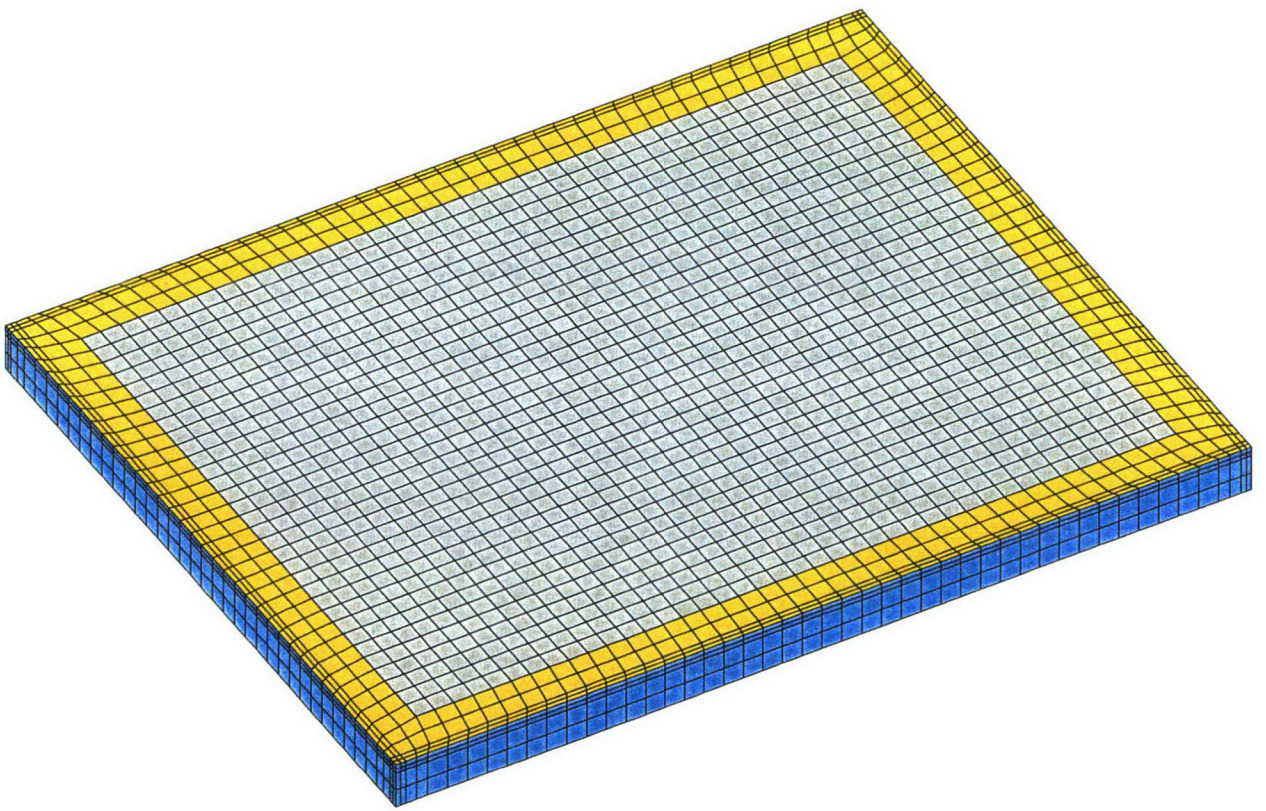

Figure 6. Finite element model of the shelf alone

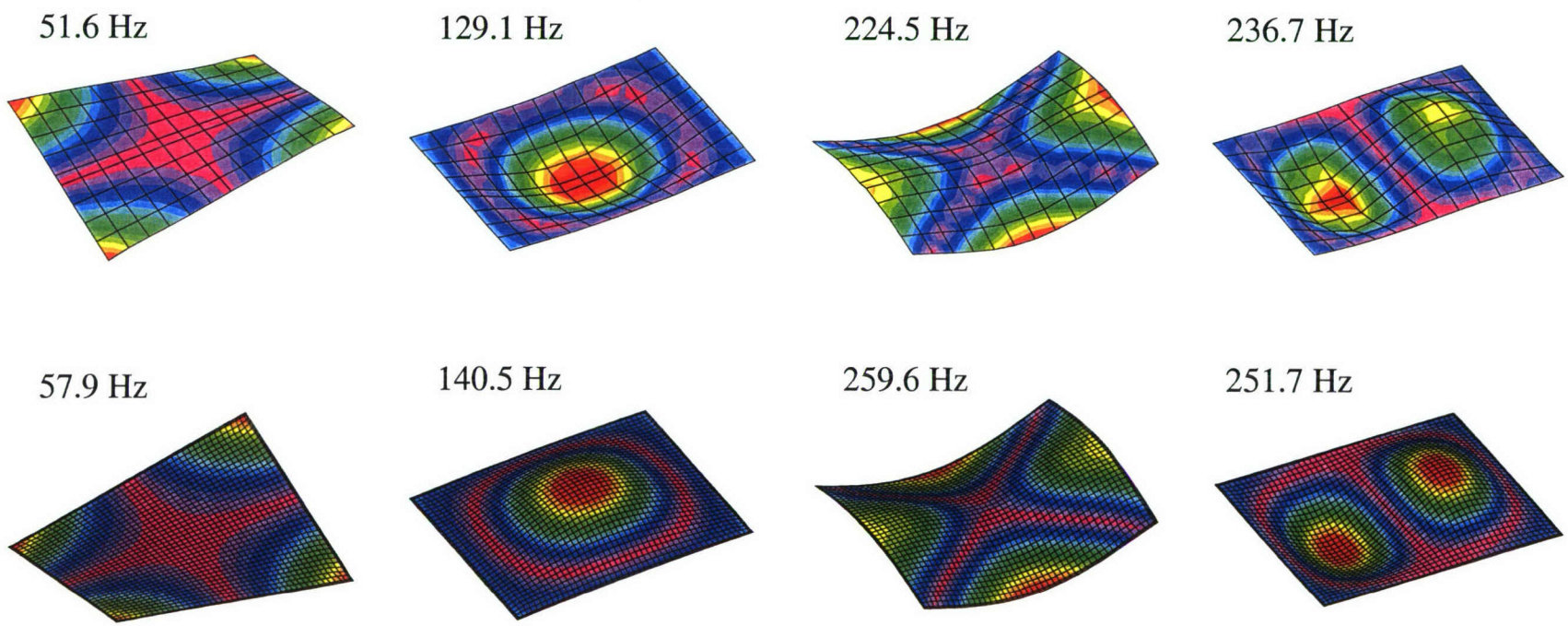

Figure 7. Comparison of the first four mode shapes for the shelf alone (top – experimental, bottom – numerical)

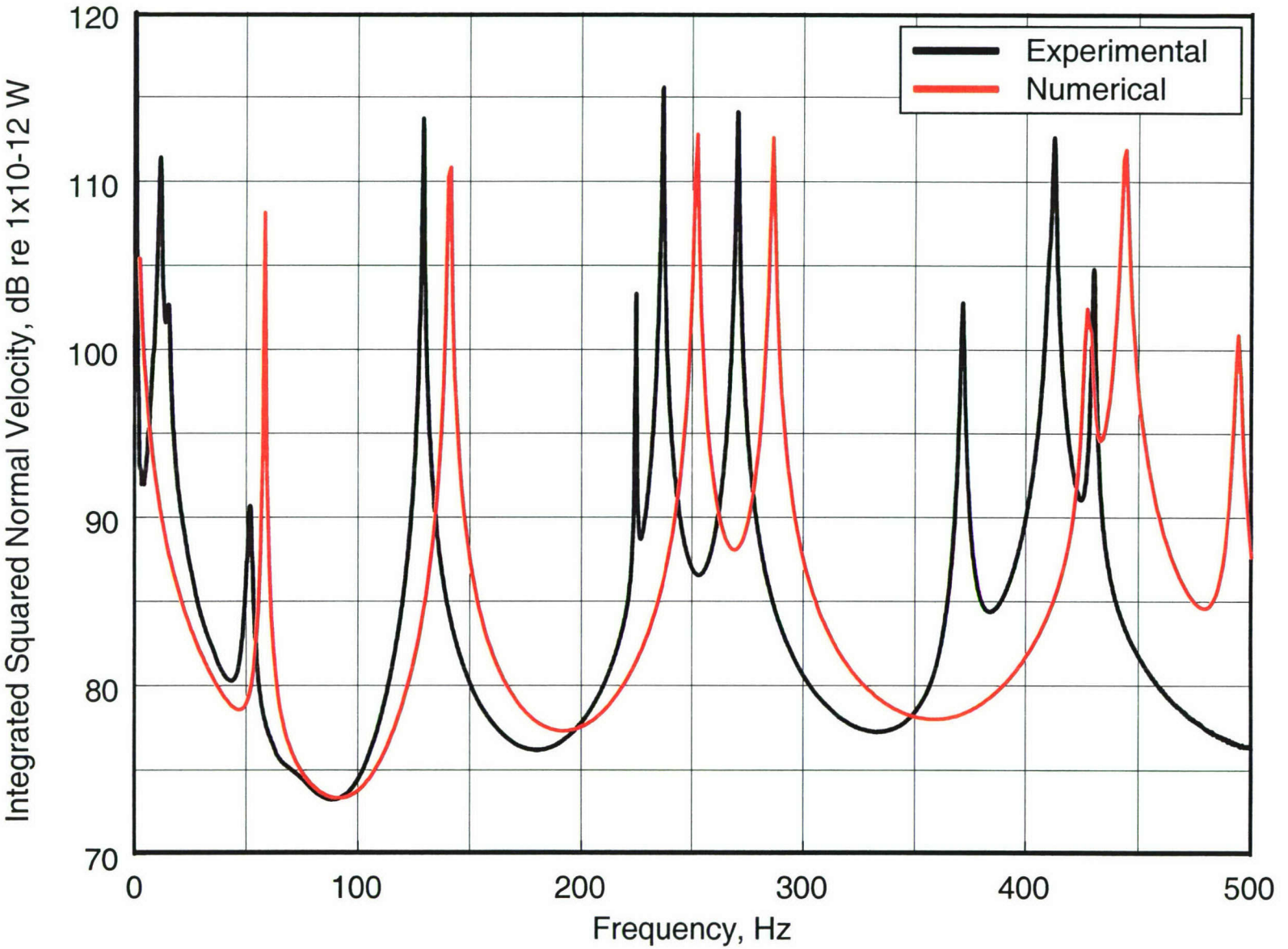

Figure 8. Comparison of the integrated squared normal velocity for the shelf alone

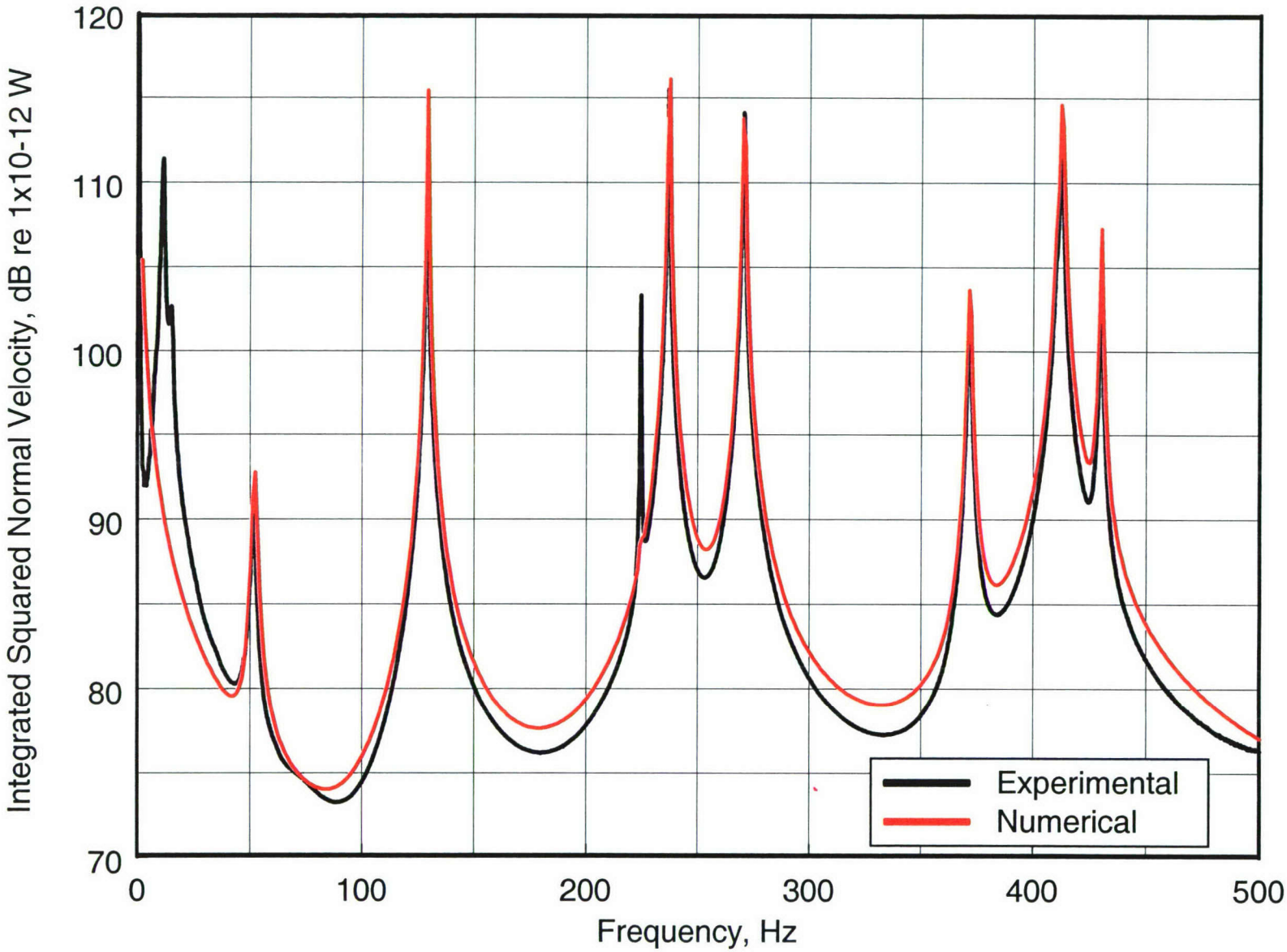

Figure 9. Integrated squared normal velocity for the shelf alone with adjusted resonance frequencies and loss factors

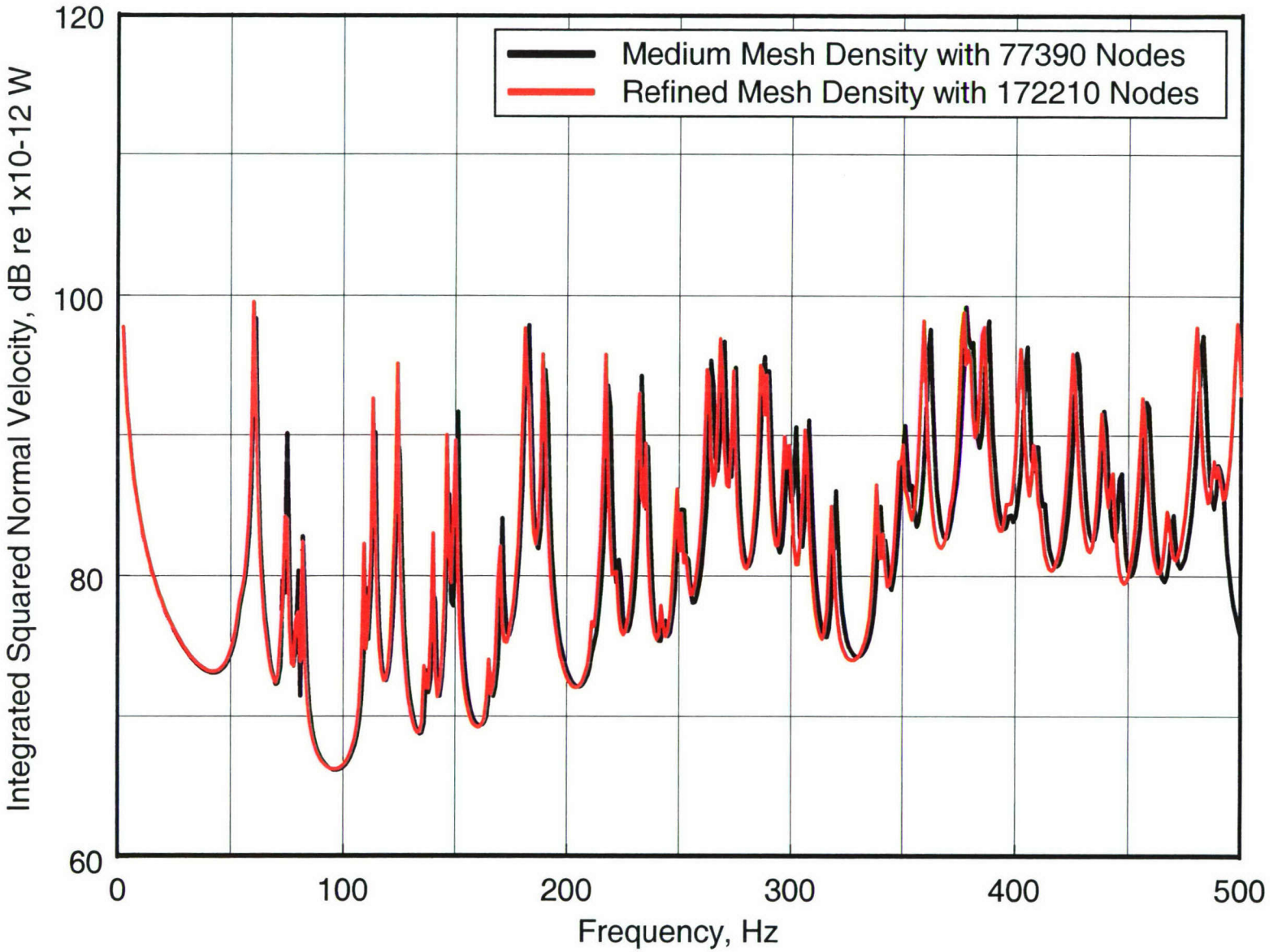

Figure 10. Convergence check for the finite element models of the enclosure without the shelf

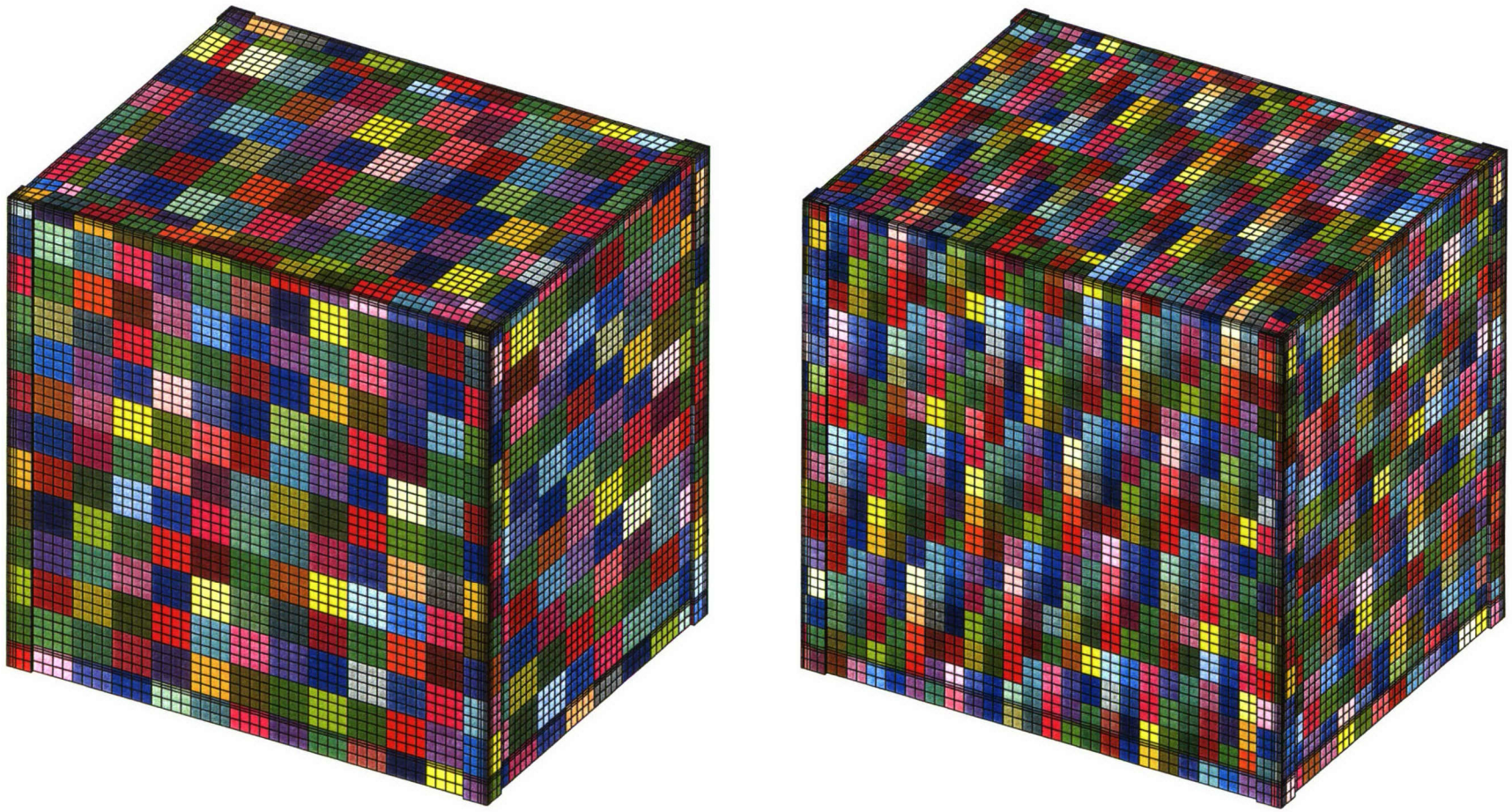

Figure 11. Acoustic meshes used to check convergence of the radiated noise predictions

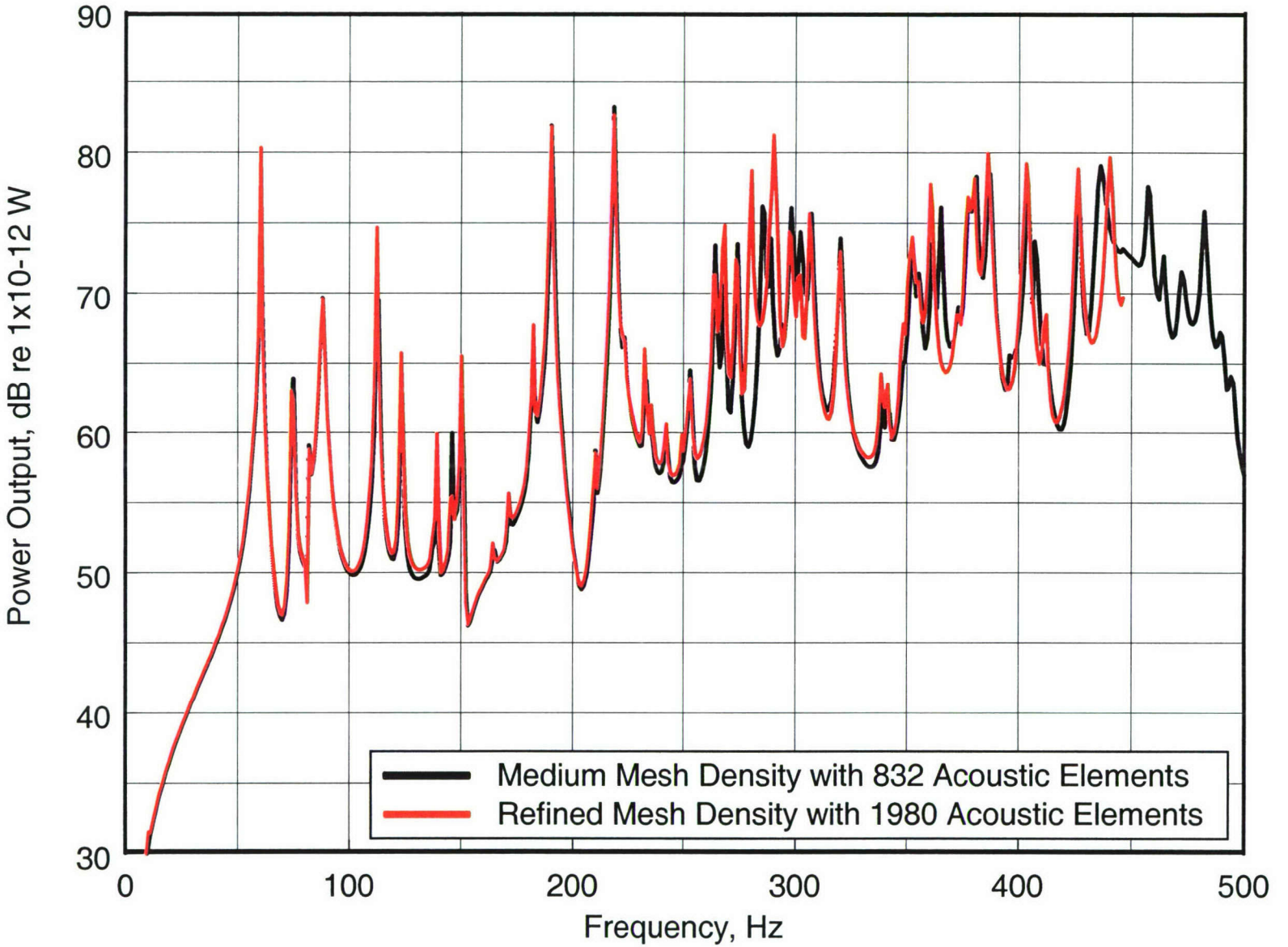

Figure 12. Convergence check for the boundary element models of the enclosure without the shelf

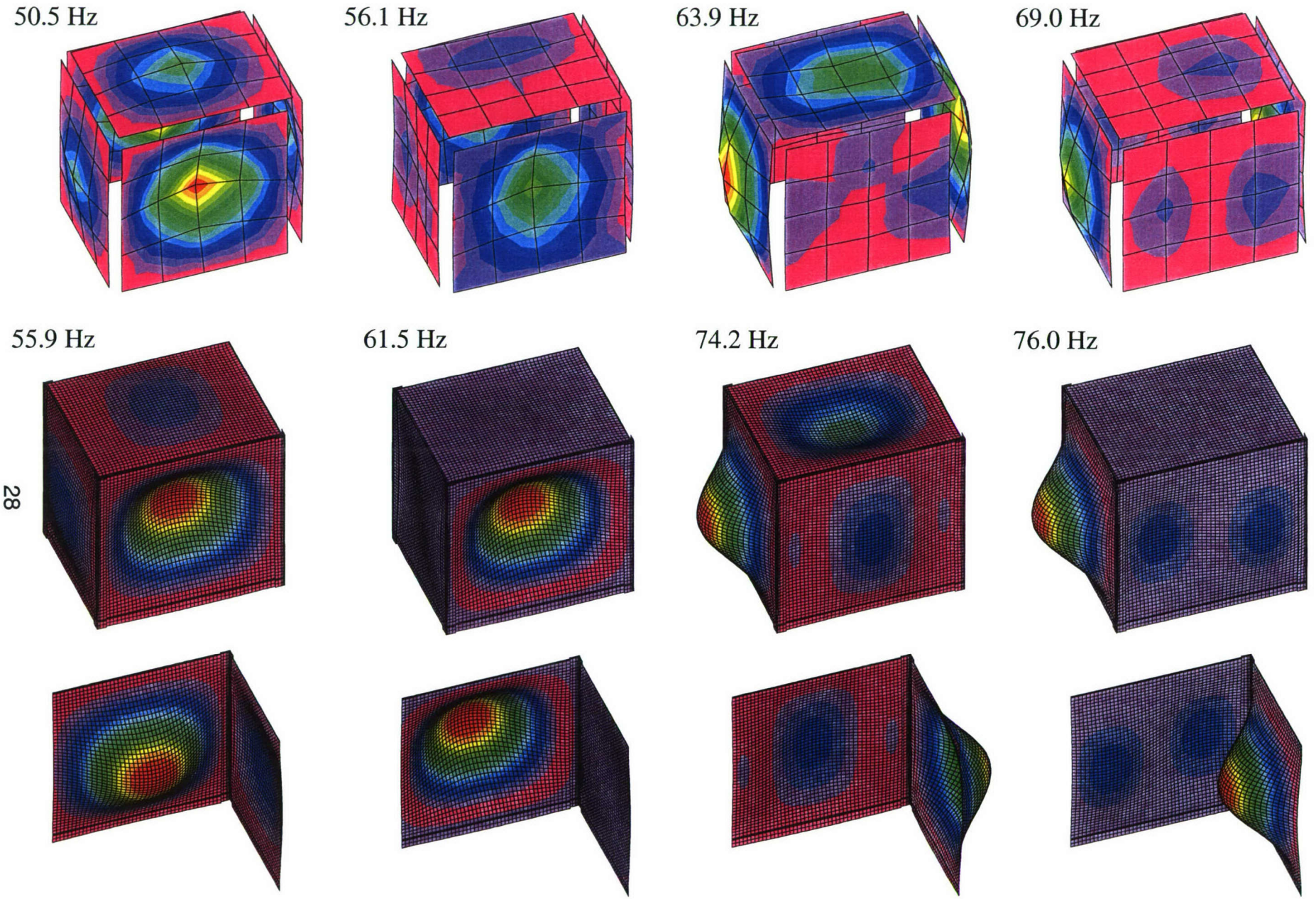

Figure 13. Comparison of the first four mode shapes for the enclosure without the shelf (top – experimental, bottom – numerical)

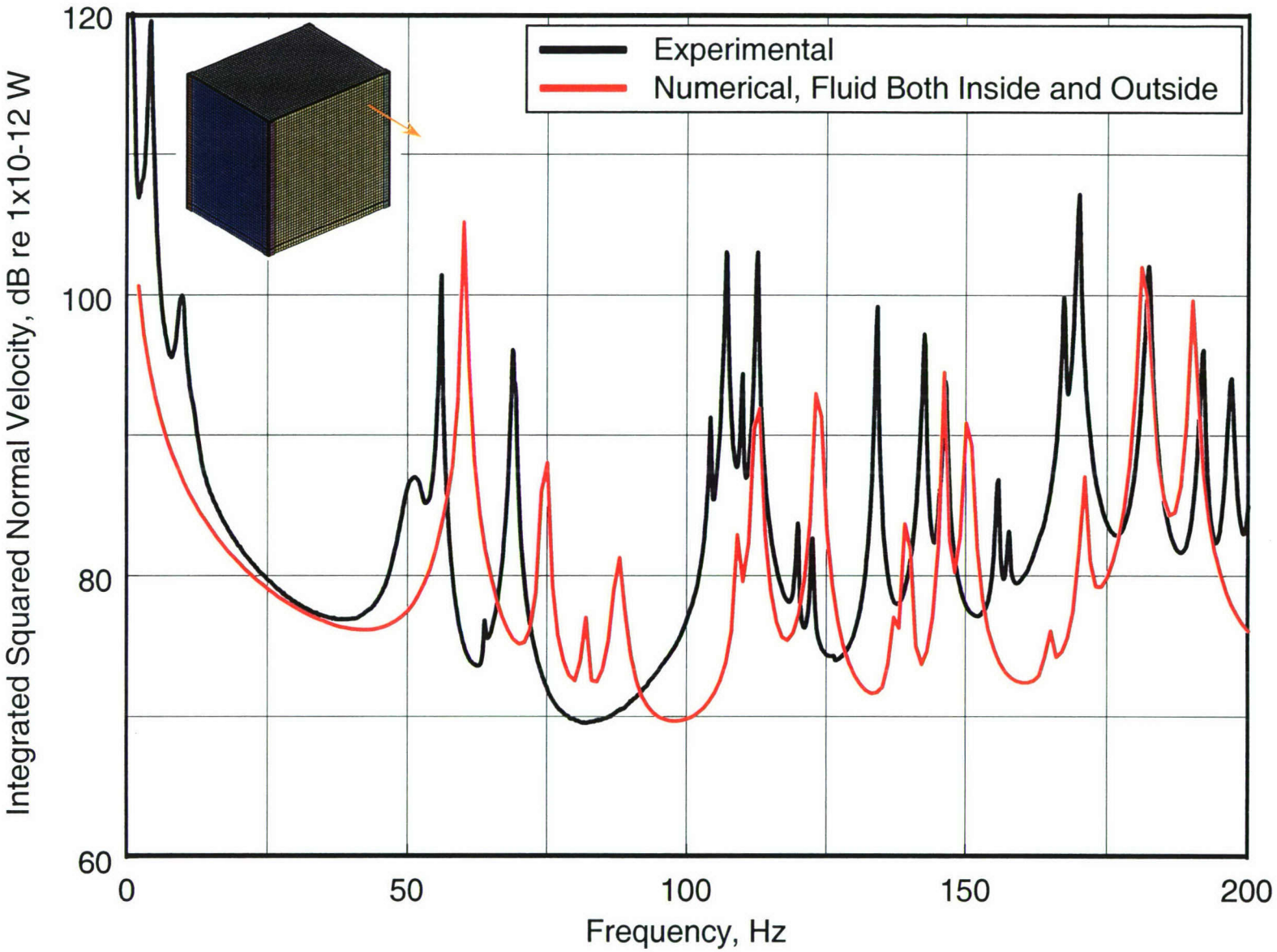

Figure 14. Experimental measurements and numerical predictions for the integrated squared normal velocity of the enclosure without the shelf

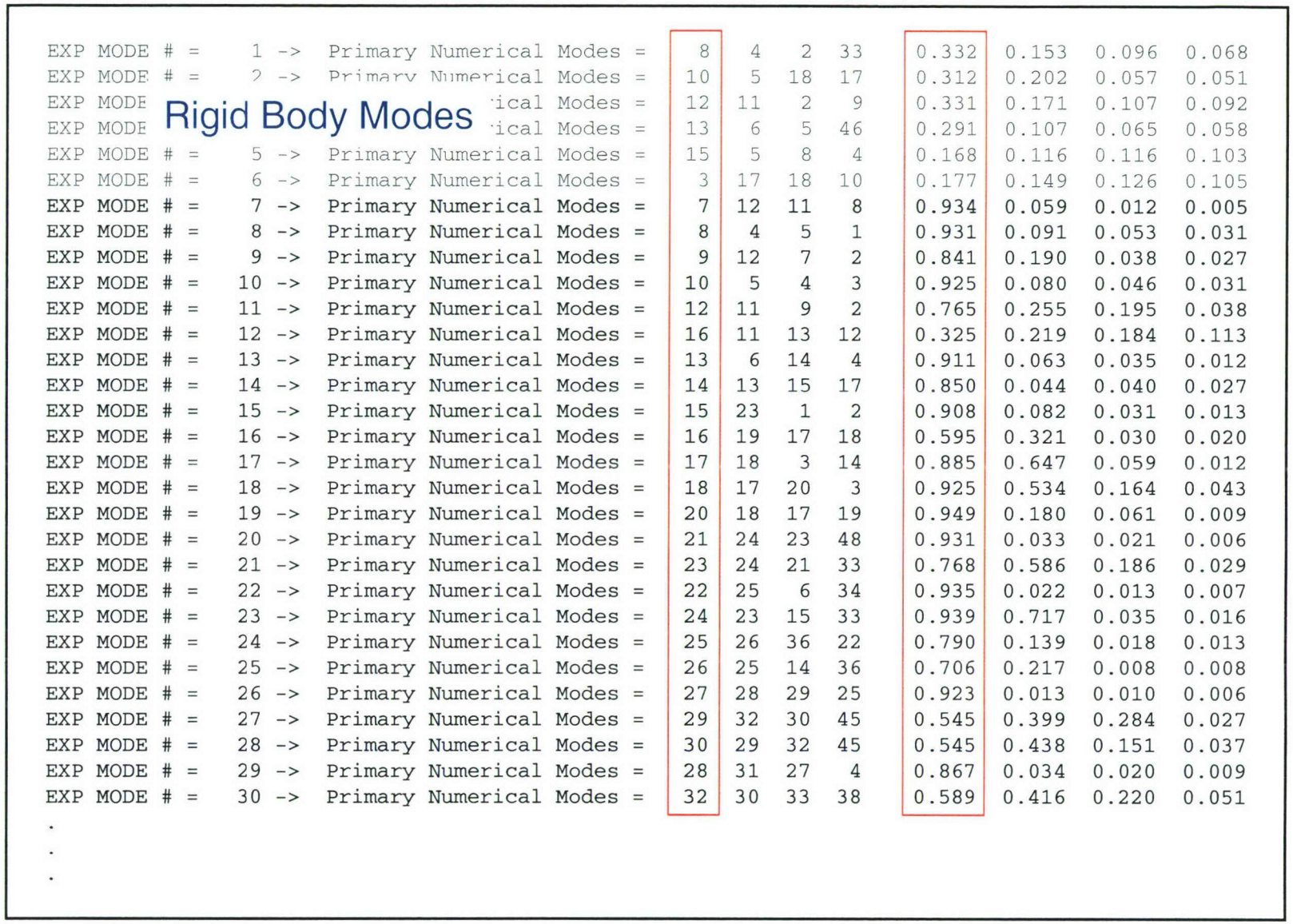


```
EXP MODE # =    1 ->  Primary Numerical Modes =   8   4   2  33   0.332  0.153  0.096  0.068
EXP MODE # =    2 ->  Primary Numerical Modes =  10   5  18  17   0.312  0.202  0.057  0.051
EXP MODE # =    3 ->  Primary Numerical Modes =  12  11   2   9   0.331  0.171  0.107  0.092
EXP MODE # =    4 ->  Primary Numerical Modes =  13   6   5  46   0.291  0.107  0.065  0.058
EXP MODE # =    5 ->  Primary Numerical Modes =  15   5   8   4   0.168  0.116  0.116  0.103
EXP MODE # =    6 ->  Primary Numerical Modes =   3  17  18  10   0.177  0.149  0.126  0.105
EXP MODE # =    7 ->  Primary Numerical Modes =   7  12  11   8   0.934  0.059  0.012  0.005
EXP MODE # =    8 ->  Primary Numerical Modes =   8   4   5   1   0.931  0.091  0.053  0.031
EXP MODE # =    9 ->  Primary Numerical Modes =   9  12   7   2   0.841  0.190  0.038  0.027
EXP MODE # =   10 ->  Primary Numerical Modes =  10   5   4   3   0.925  0.080  0.046  0.031
EXP MODE # =   11 ->  Primary Numerical Modes =  12  11   9   2   0.765  0.255  0.195  0.038
EXP MODE # =   12 ->  Primary Numerical Modes =  16  11  13  12   0.325  0.219  0.184  0.113
EXP MODE # =   13 ->  Primary Numerical Modes =  13   6  14   4   0.911  0.063  0.035  0.012
EXP MODE # =   14 ->  Primary Numerical Modes =  14  13  15  17   0.850  0.044  0.040  0.027
EXP MODE # =   15 ->  Primary Numerical Modes =  15  23   1   2   0.908  0.082  0.031  0.013
EXP MODE # =   16 ->  Primary Numerical Modes =  16  19  17  18   0.595  0.321  0.030  0.020
EXP MODE # =   17 ->  Primary Numerical Modes =  17  18   3  14   0.885  0.647  0.059  0.012
EXP MODE # =   18 ->  Primary Numerical Modes =  18  17  20   3   0.925  0.534  0.164  0.043
EXP MODE # =   19 ->  Primary Numerical Modes =  20  18  17  19   0.949  0.180  0.061  0.009
EXP MODE # =   20 ->  Primary Numerical Modes =  21  24  23  48   0.931  0.033  0.021  0.006
EXP MODE # =   21 ->  Primary Numerical Modes =  23  24  21  33   0.768  0.586  0.186  0.029
EXP MODE # =   22 ->  Primary Numerical Modes =  22  25   6  34   0.935  0.022  0.013  0.007
EXP MODE # =   23 ->  Primary Numerical Modes =  24  23  15  33   0.939  0.717  0.035  0.016
EXP MODE # =   24 ->  Primary Numerical Modes =  25  26  36  22   0.790  0.139  0.018  0.013
EXP MODE # =   25 ->  Primary Numerical Modes =  26  25  14  36   0.706  0.217  0.008  0.008
EXP MODE # =   26 ->  Primary Numerical Modes =  27  28  29  25   0.923  0.013  0.010  0.006
EXP MODE # =   27 ->  Primary Numerical Modes =  29  32  30  45   0.545  0.399  0.284  0.027
EXP MODE # =   28 ->  Primary Numerical Modes =  30  29  32  45   0.545  0.438  0.151  0.037
EXP MODE # =   29 ->  Primary Numerical Modes =  28  31  27   4   0.867  0.034  0.020  0.009
EXP MODE # =   30 ->  Primary Numerical Modes =  32  30  33  38   0.589  0.416  0.220  0.051
.
.
.
```

Figure 15. Sample output from the MAC analysis of the enclosure without the shelf

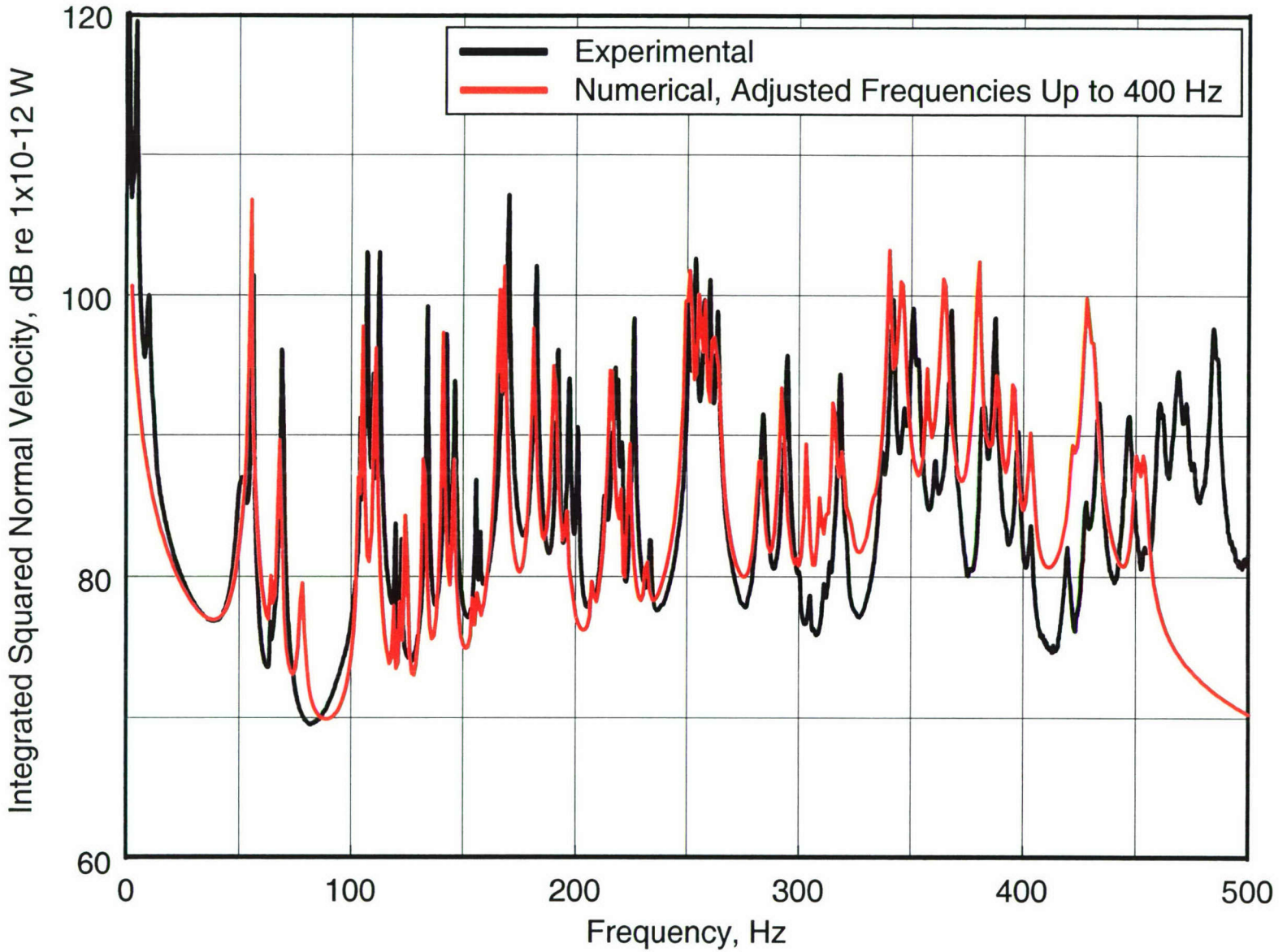

Figure 16. Experimental measurements and numerical predictions for the integrated squared normal velocity of the enclosure without the shelf

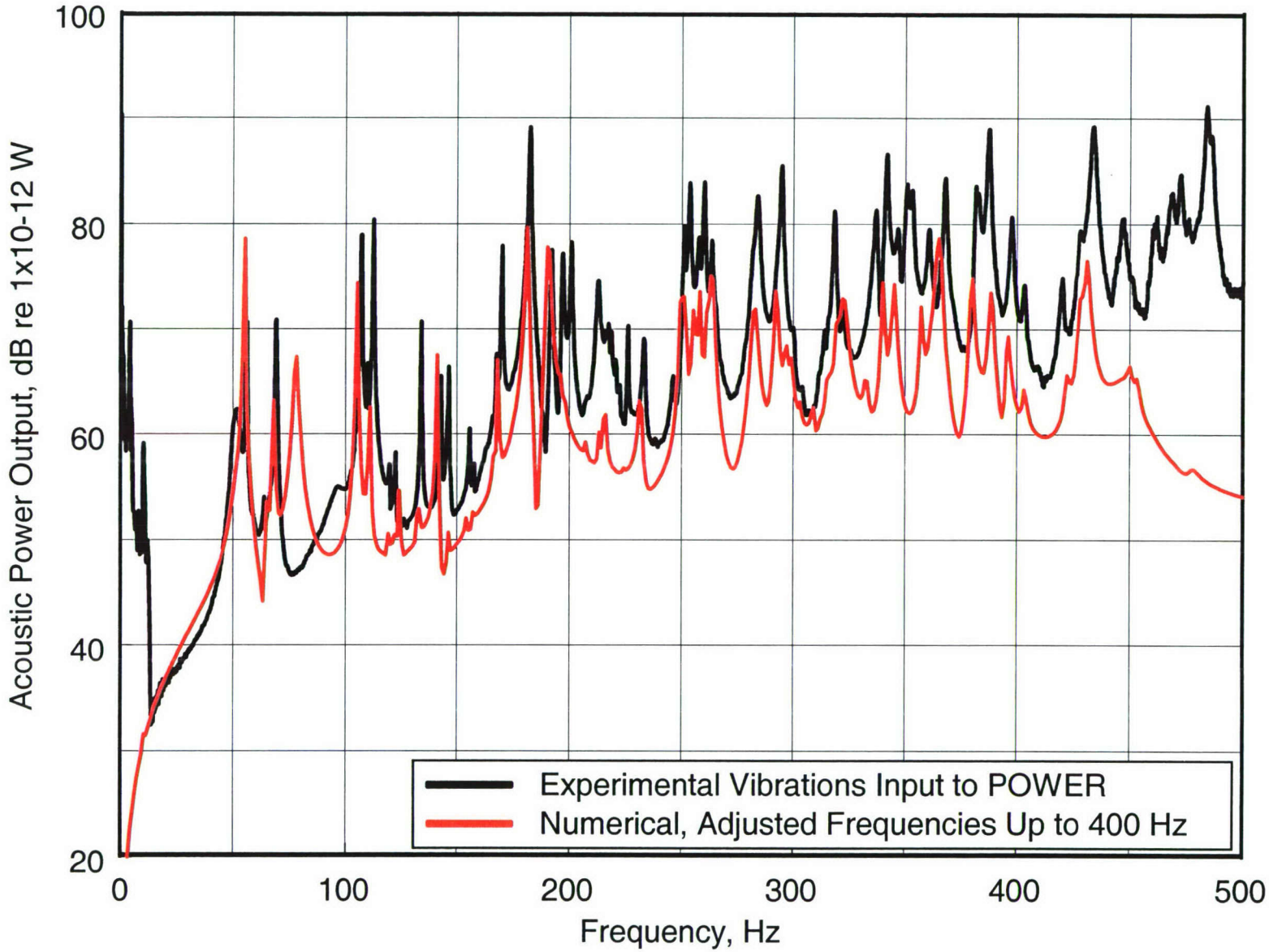

Figure 17. Numerical predictions for the acoustic power output of the enclosure without the shelf

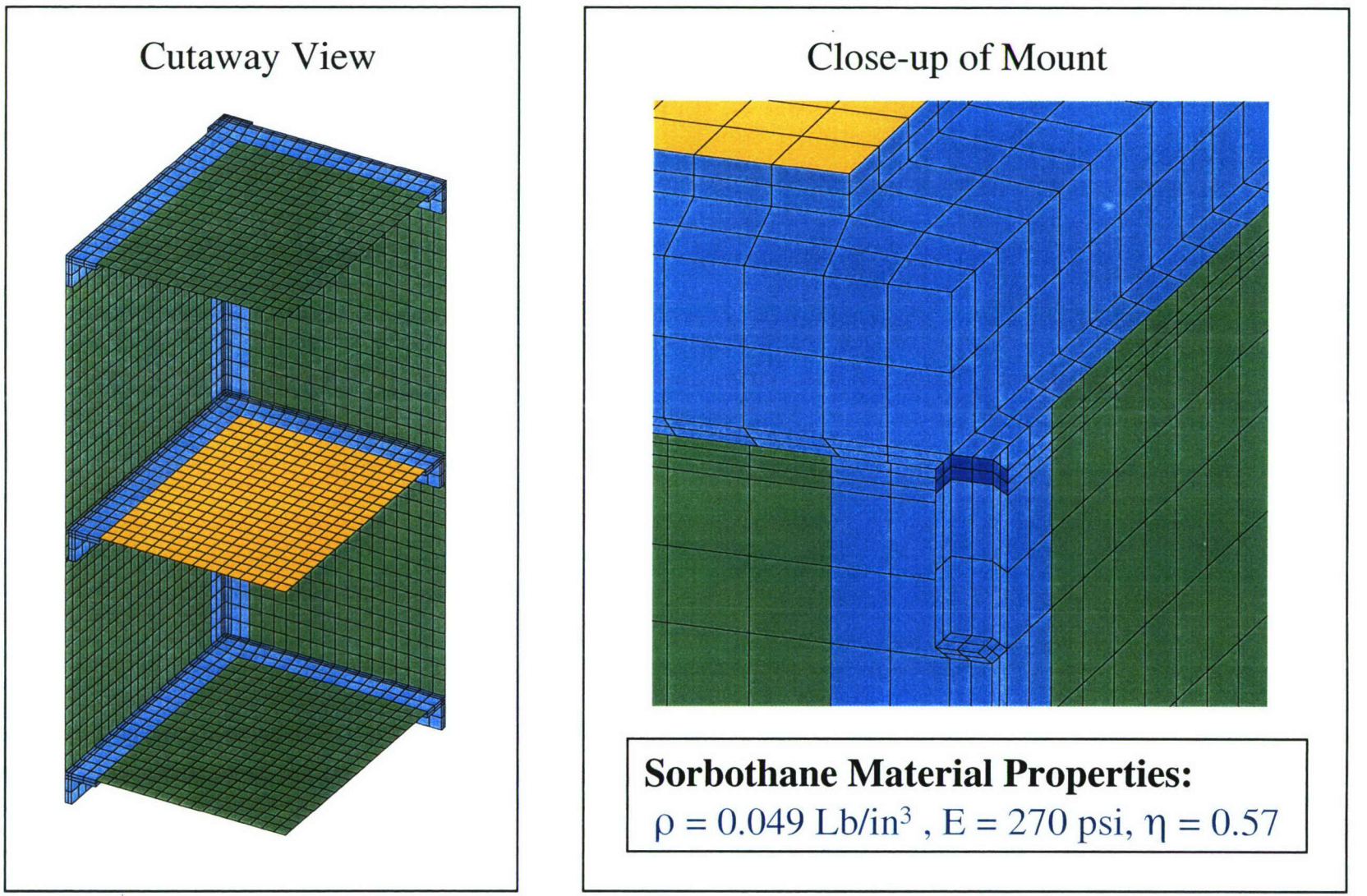

Figure 18. Illustrations of the finite element model with the shelf resting on sorbothane

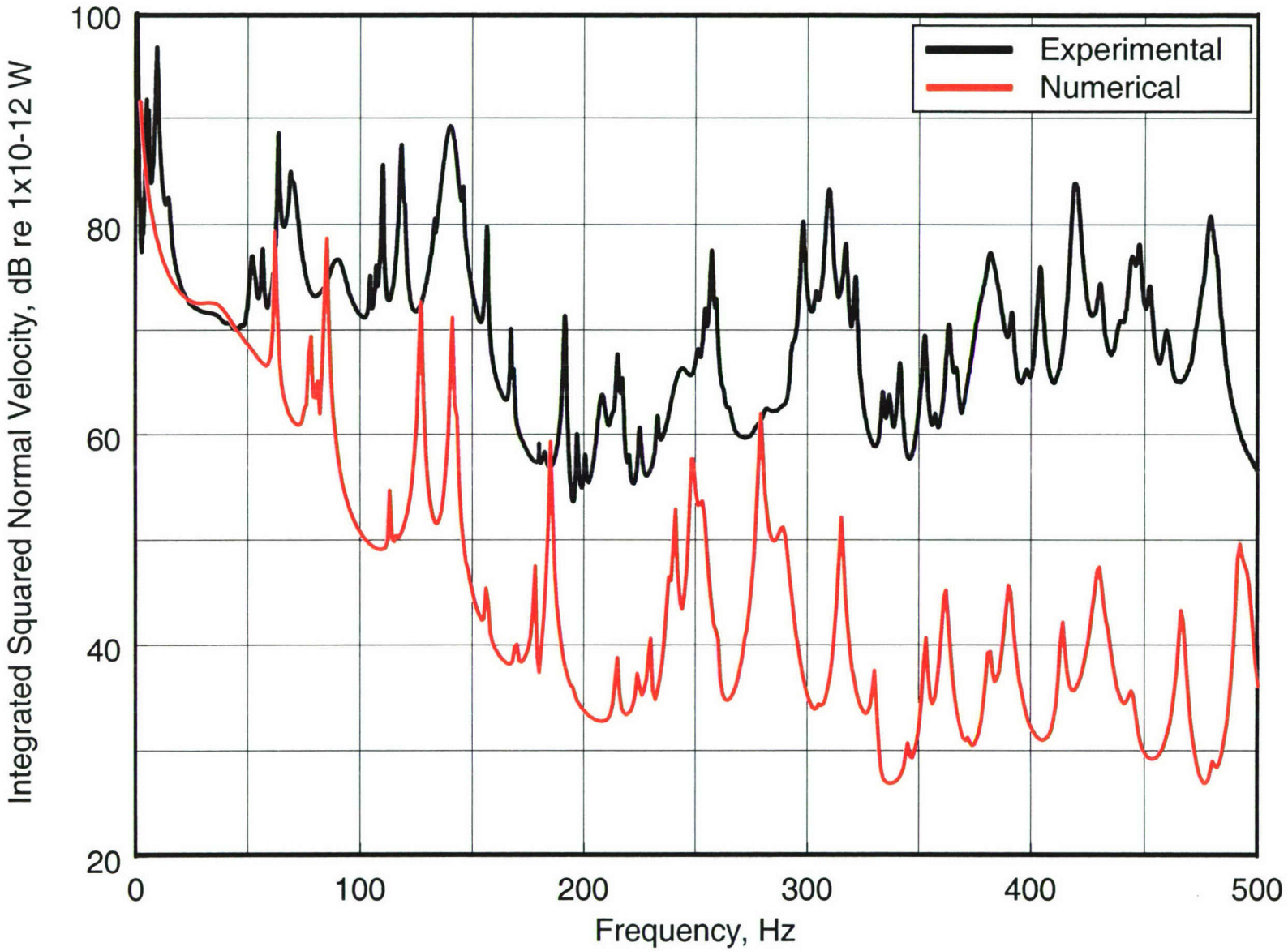

Figure 19. Experimental measurements and numerical predictions for the integrated squared normal velocity of the enclosure with the shelf resting on sorbothane

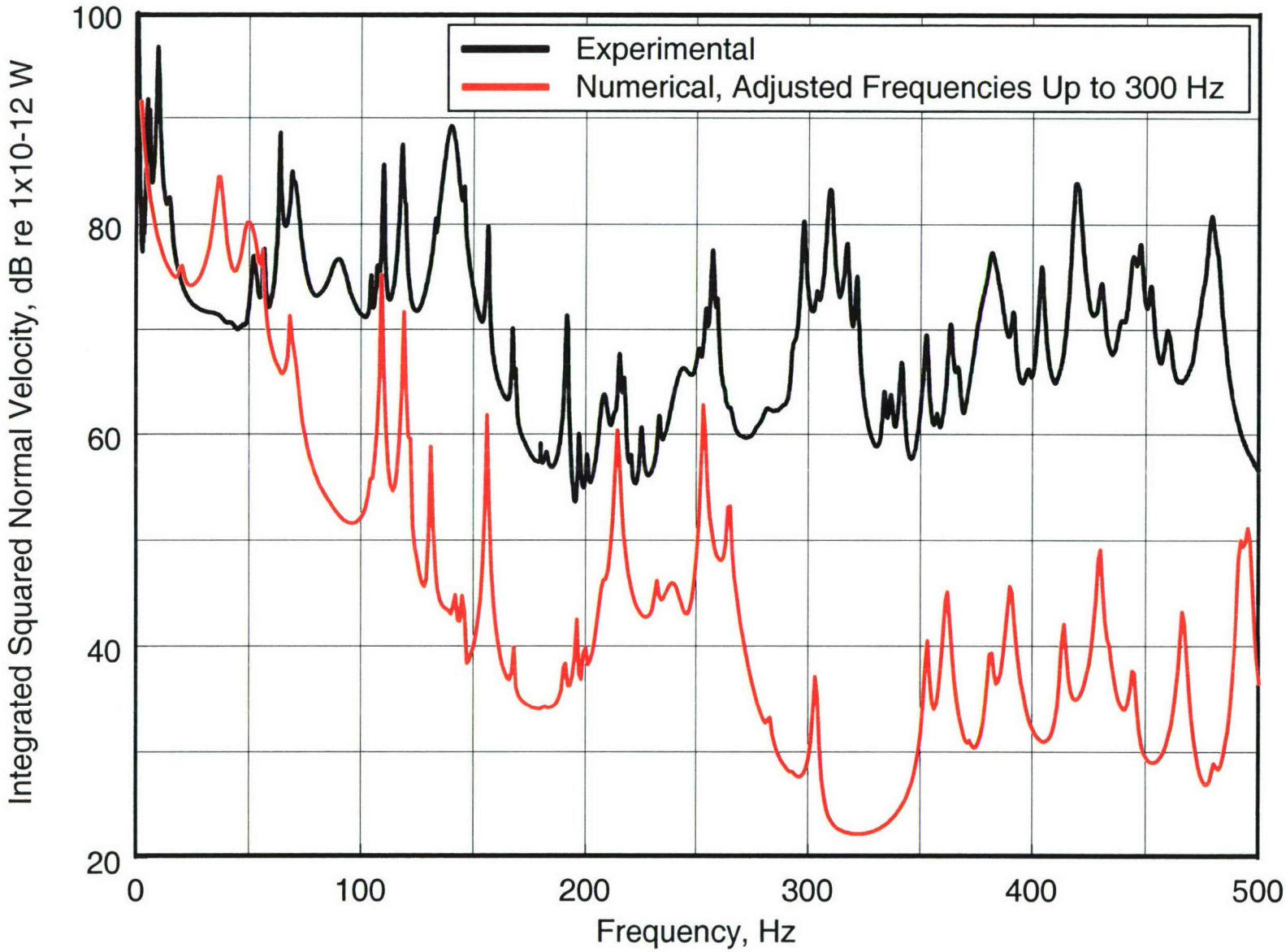

Figure 20. Experimental measurements and numerical predictions for the integrated squared normal velocity of the enclosure with the shelf resting on sorbothane

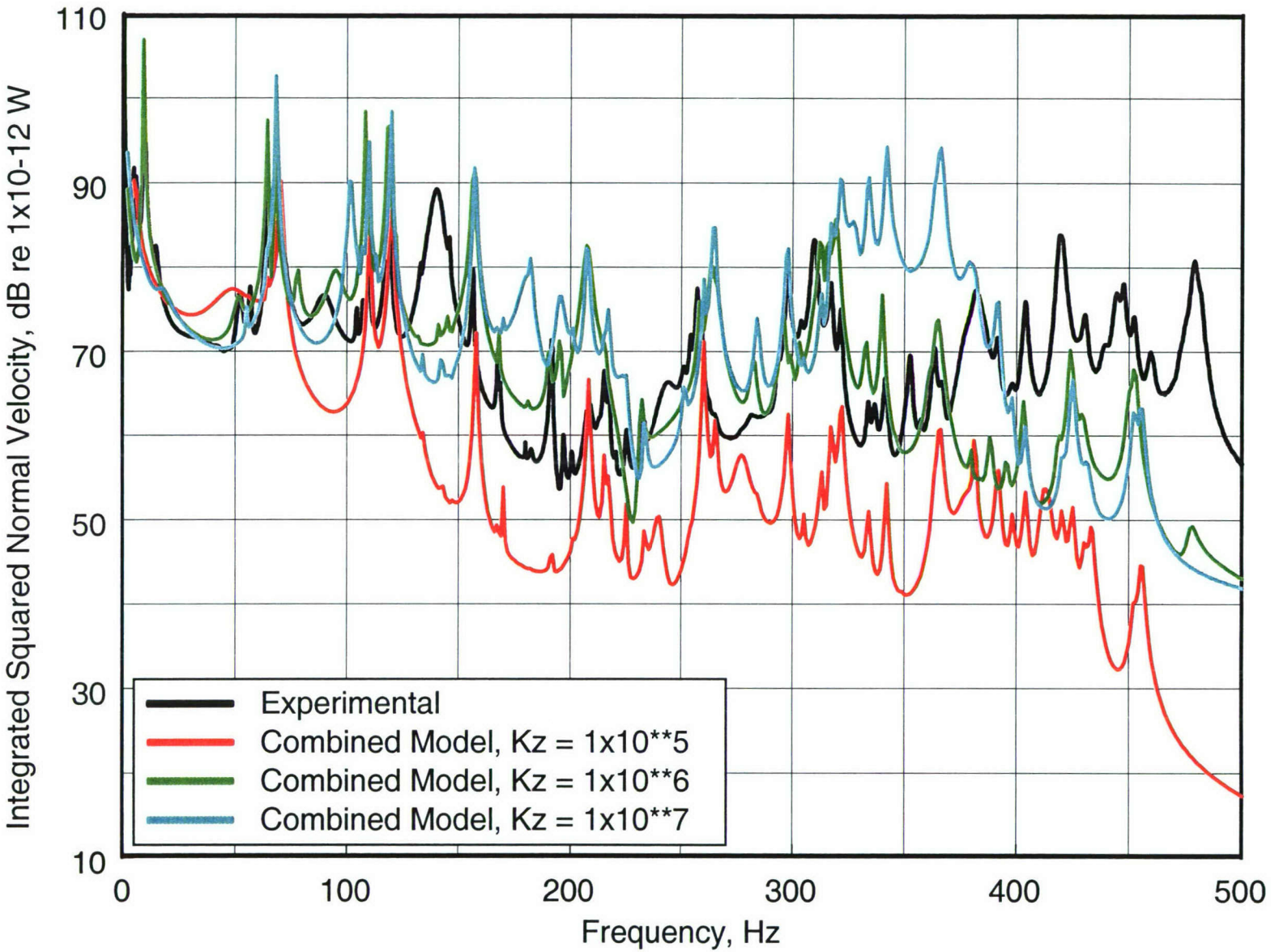

Figure 21. Experimental measurements and numerical predictions for the integrated squared normal velocity of the enclosure with the shelf resting on sorbothane

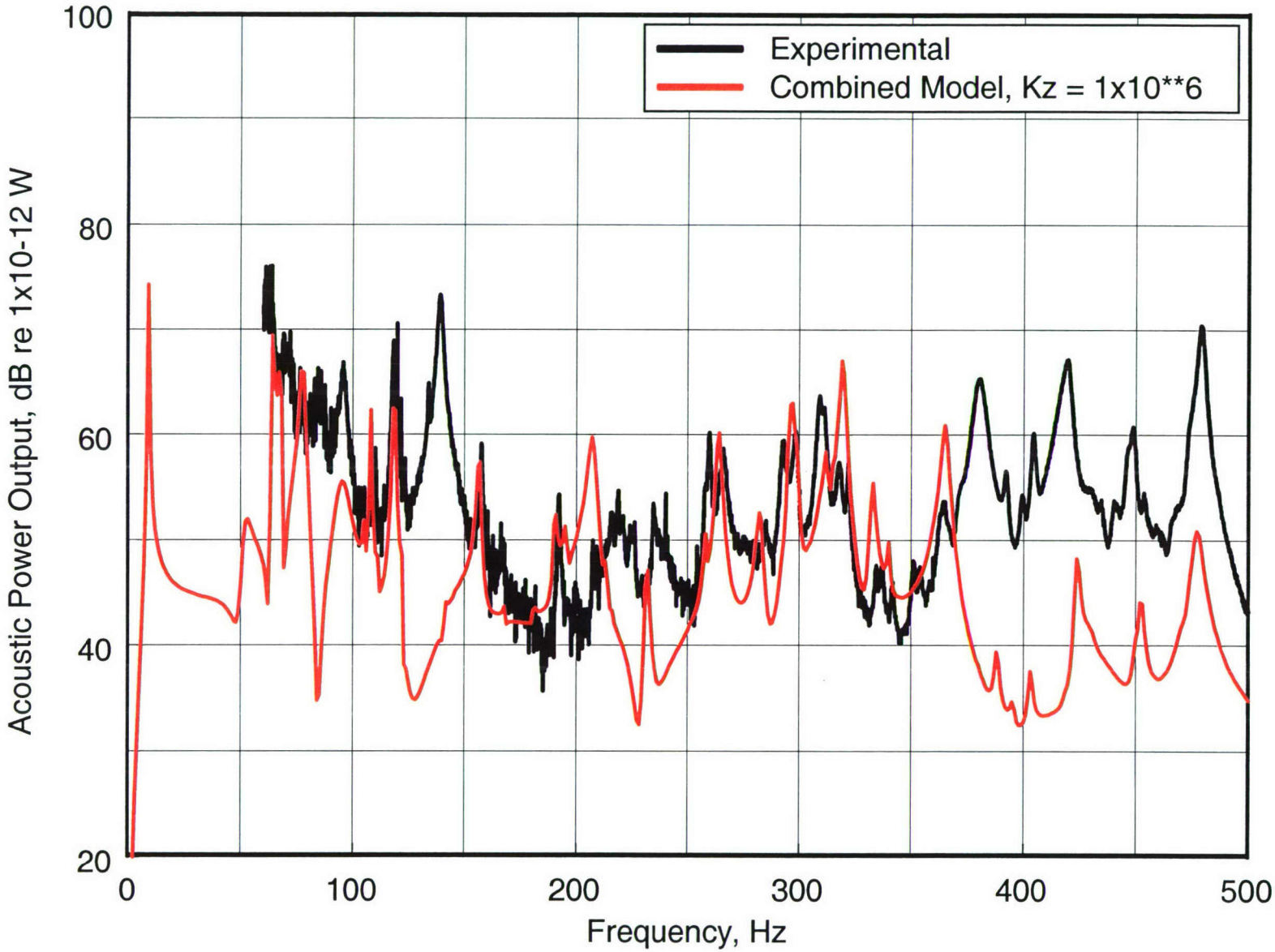

Figure 22. Experimental measurements and numerical predictions for the acoustic power output with the shelf resting on sorbothane

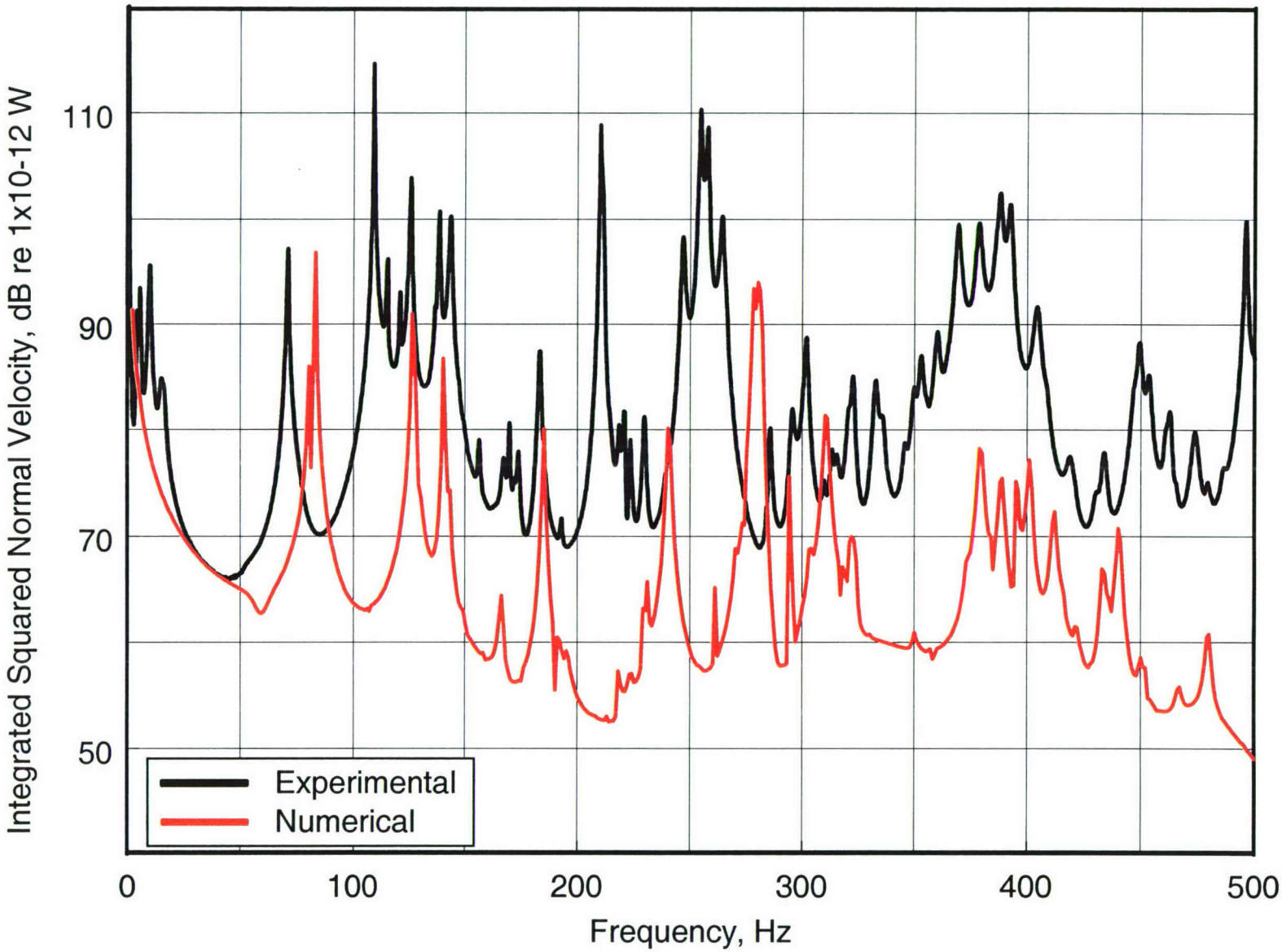

Figure 23. Experimental measurements and numerical predictions for the integrated squared normal velocity of the enclosure with the shelf hinged

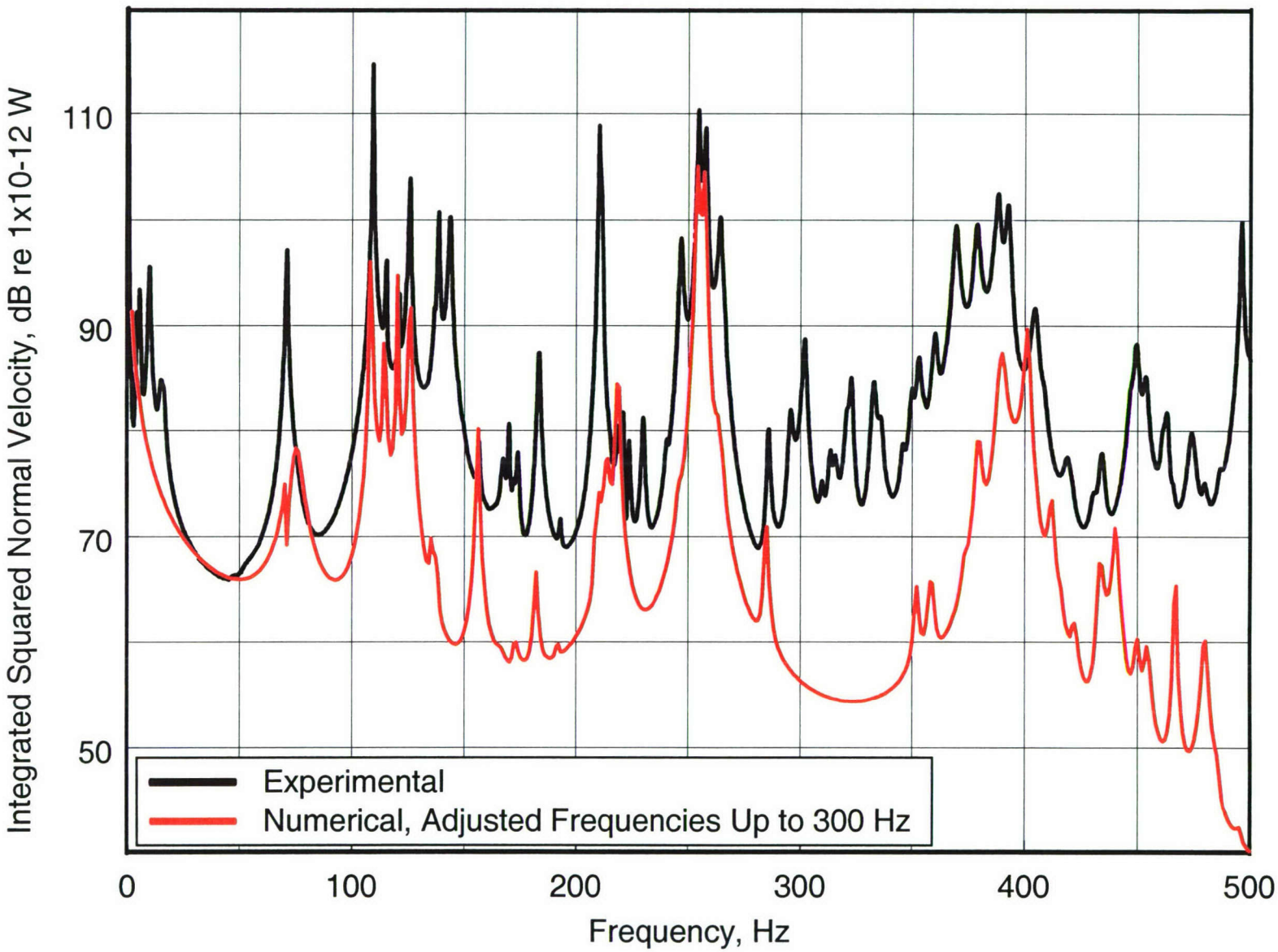

Figure 24. Experimental measurements and numerical predictions for the integrated squared normal velocity of the enclosure with the shelf hinged

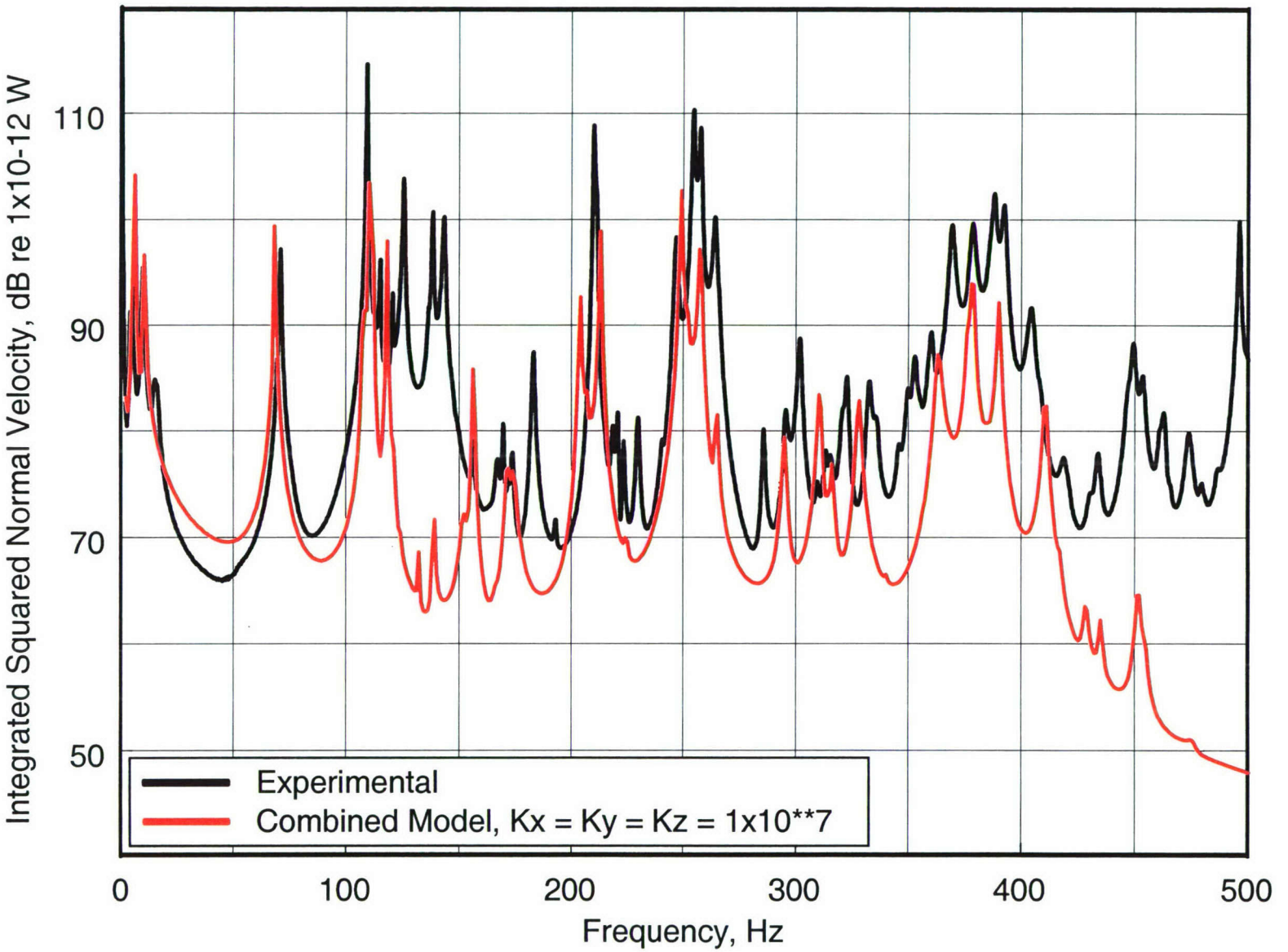

Figure 25. Experimental measurements and numerical predictions for the integrated squared normal velocity of the enclosure with the shelf hinged

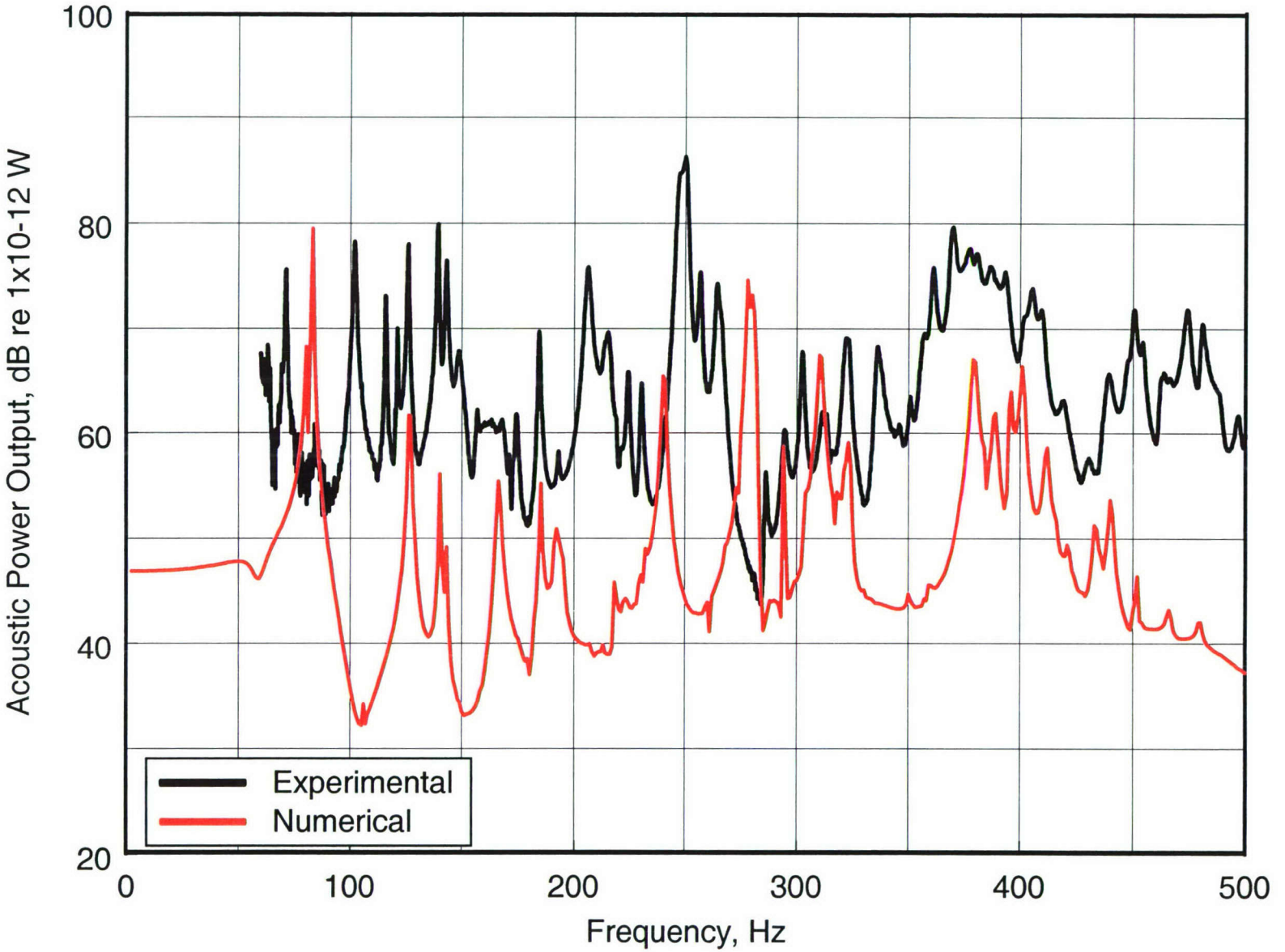

Figure 26. Experimental measurements and numerical predictions for the acoustic power output with the shelf hinged.

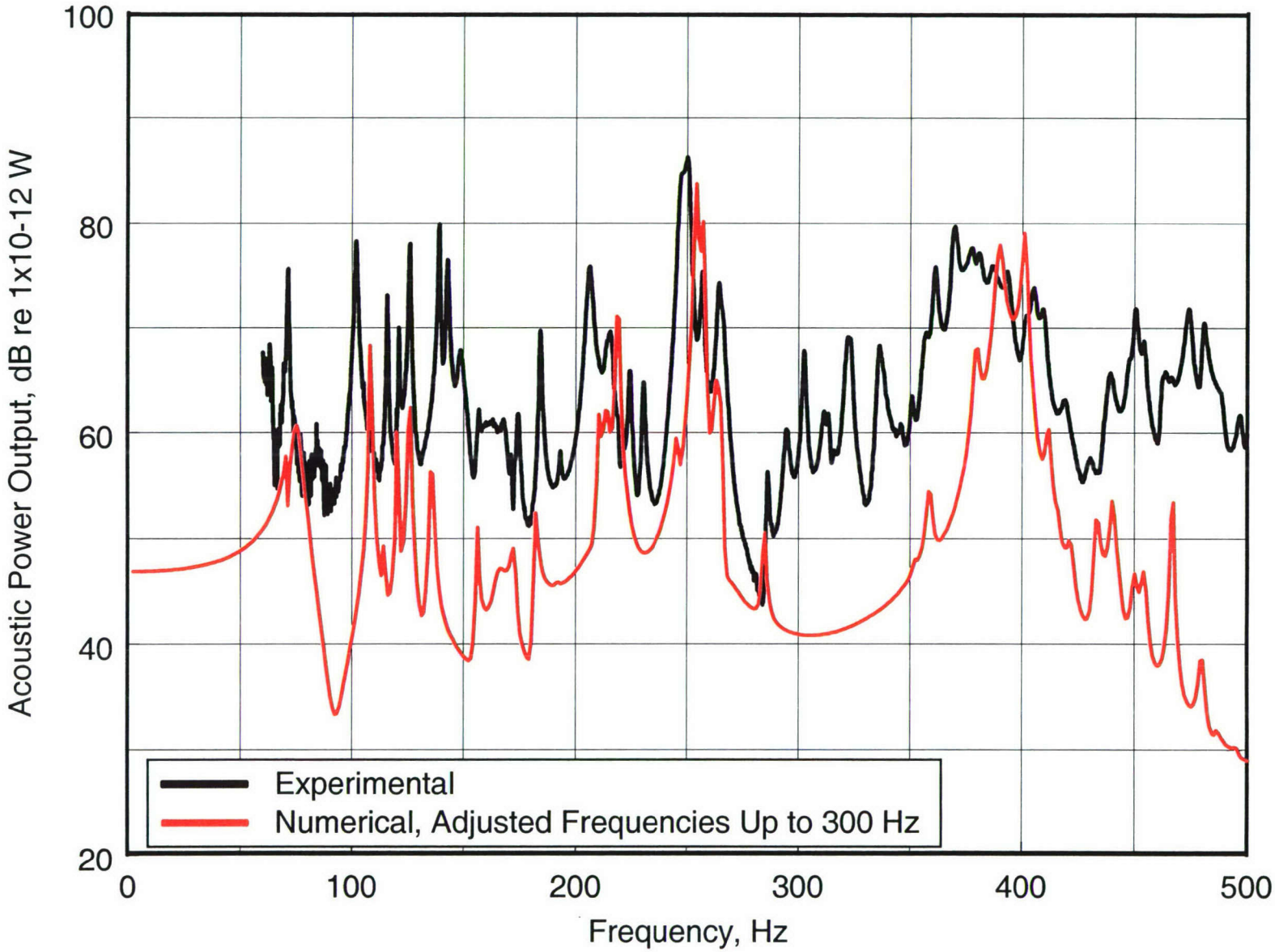

Figure 27. Experimental measurements and numerical predictions for the acoustic power output with the shelf hinged

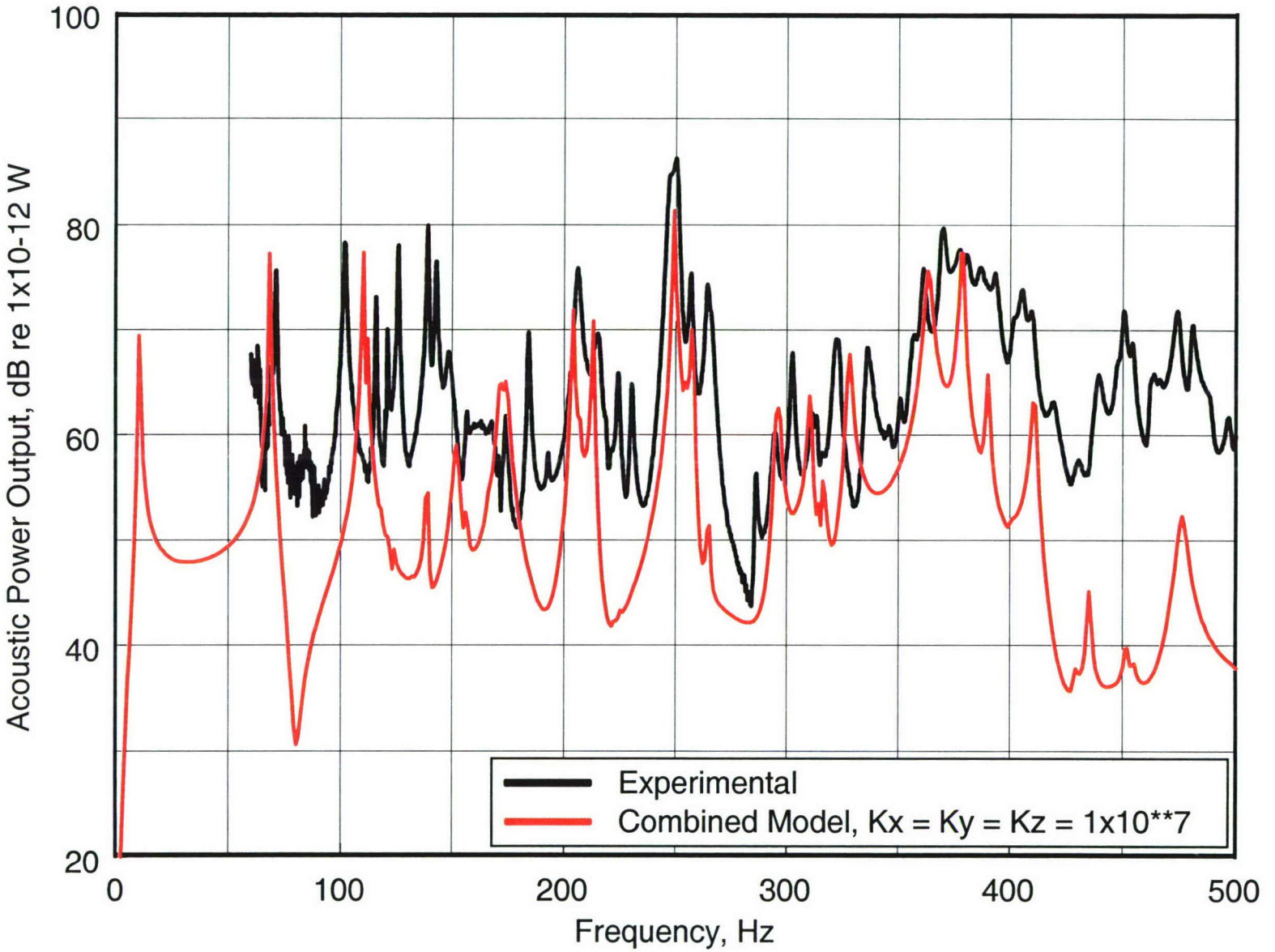

Figure 28. Experimental measurements and numerical predictions for the acoustic power output with the shelf hinged

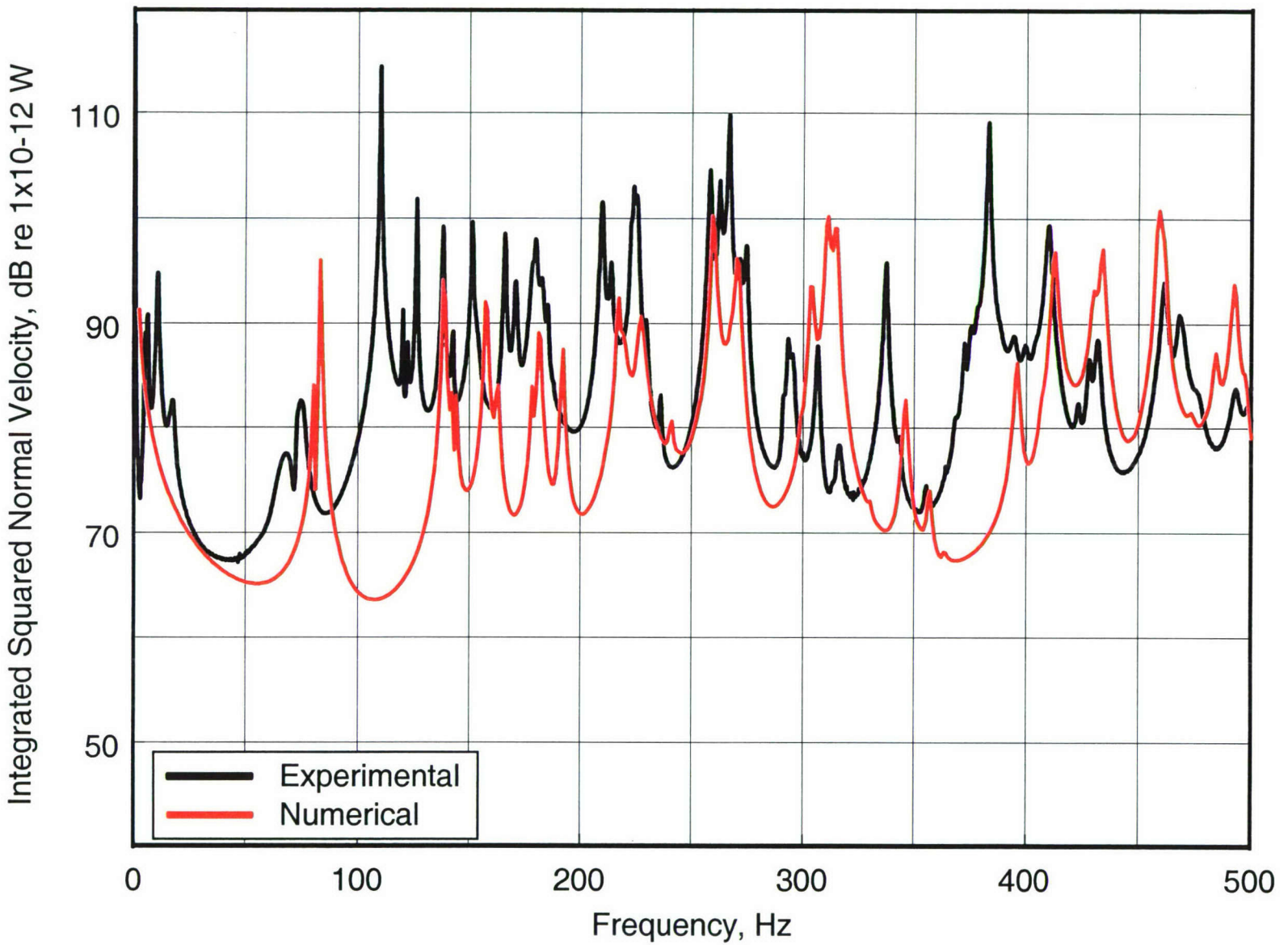

Figure 29. Experimental measurements and numerical predictions for the integrated squared normal velocity of the enclosure with the shelf clamped

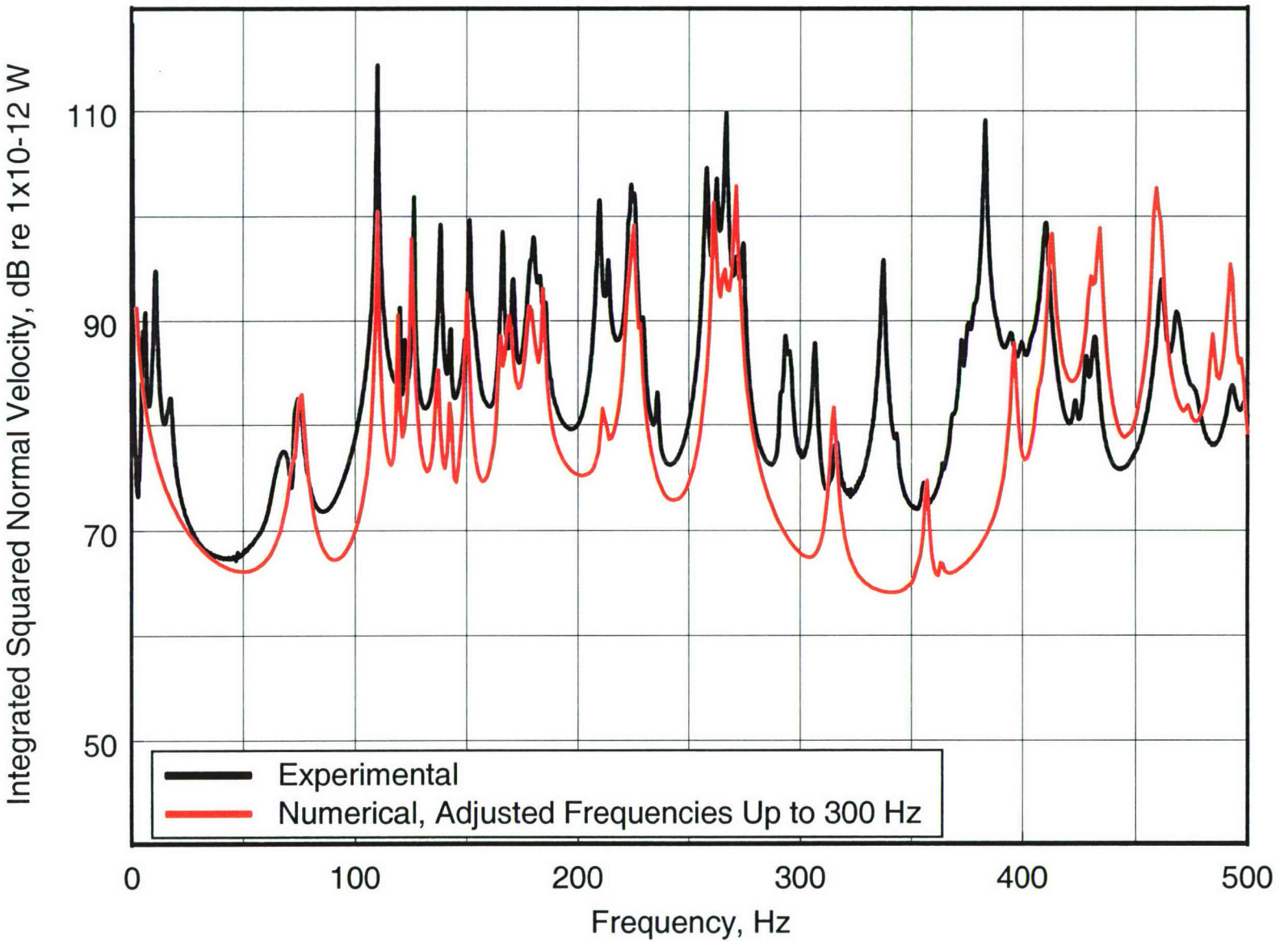

Figure 30. Experimental measurements and numerical predictions for the integrated squared normal velocity of the enclosure with the shelf clamped

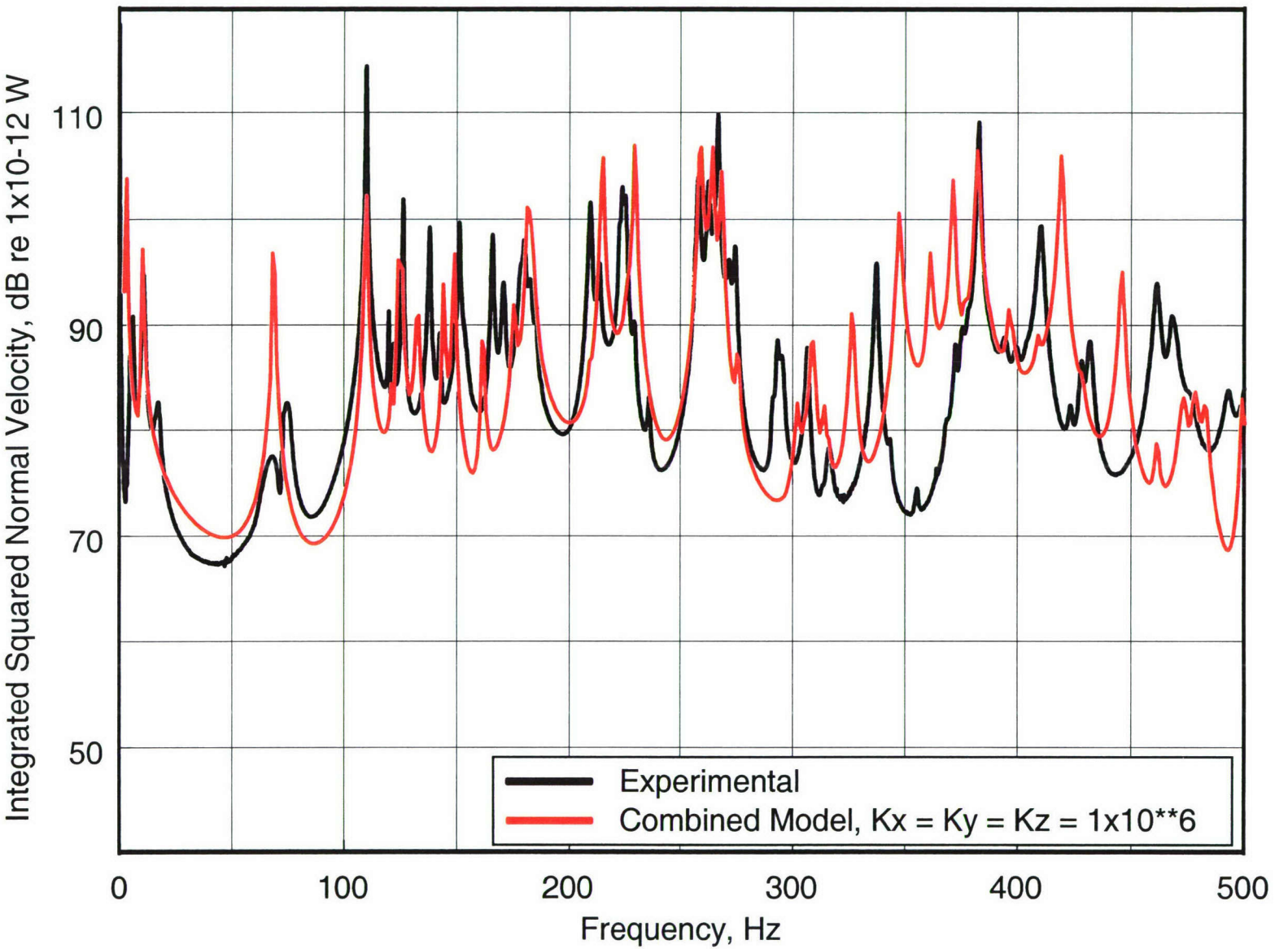

Figure 31. Experimental measurements and numerical predictions for the integrated squared normal velocity of the enclosure with the shelf clamped

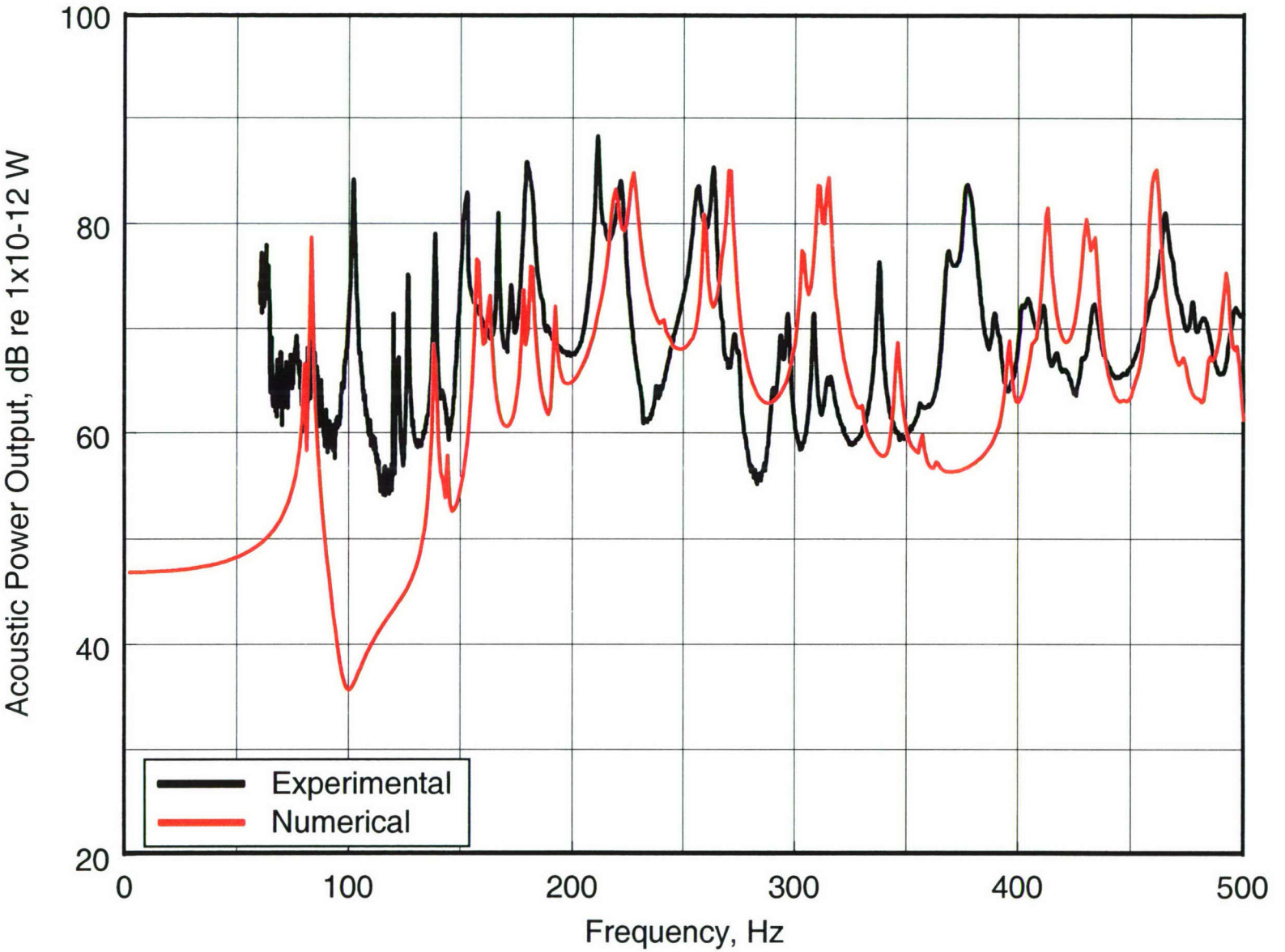

Figure 32. Experimental measurements and numerical predictions for the acoustic power output of the enclosure with the shelf clamped

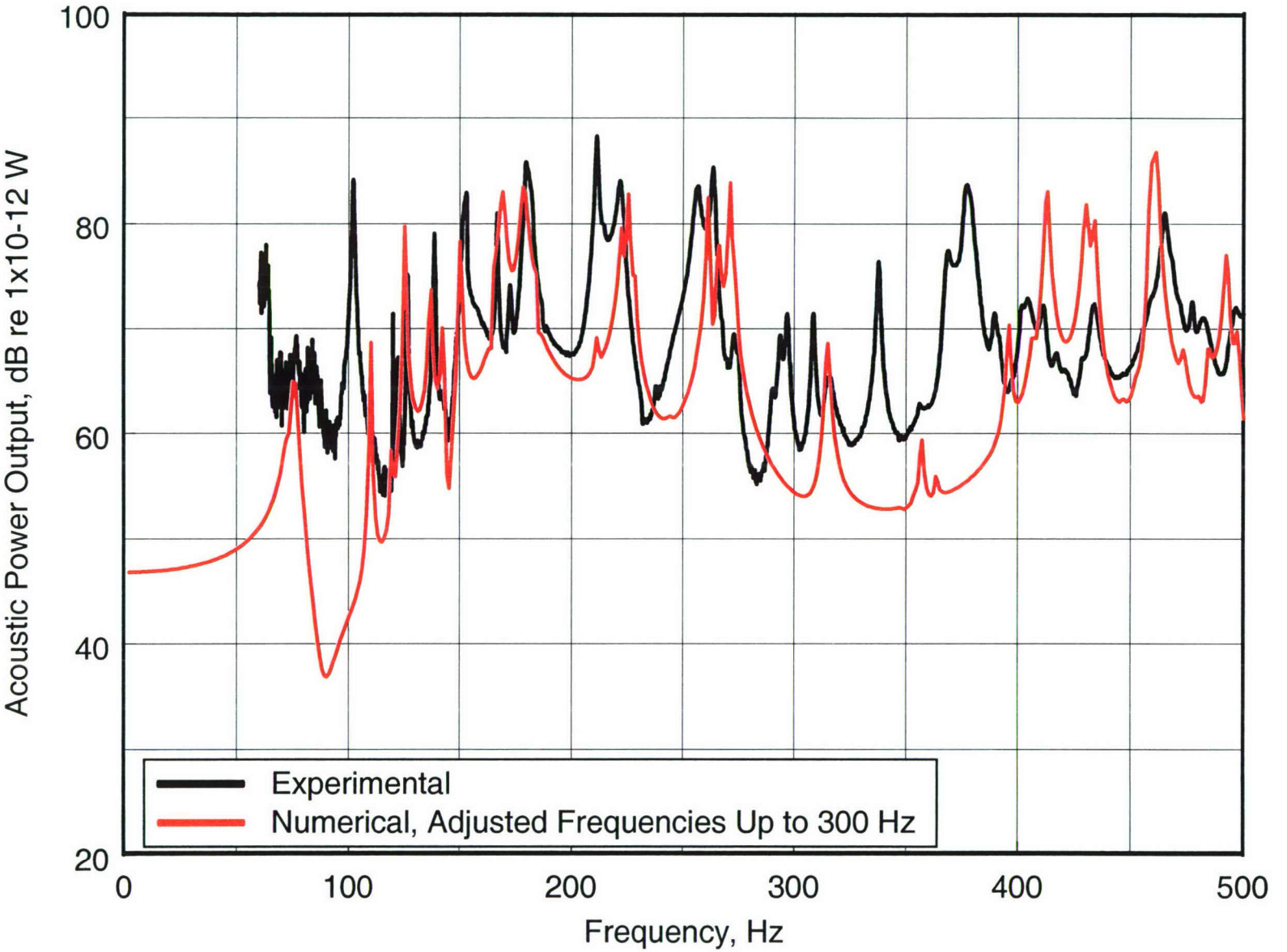

Figure 33. Experimental measurements and numerical predictions for the acoustic power output of the enclosure with the shelf clamped

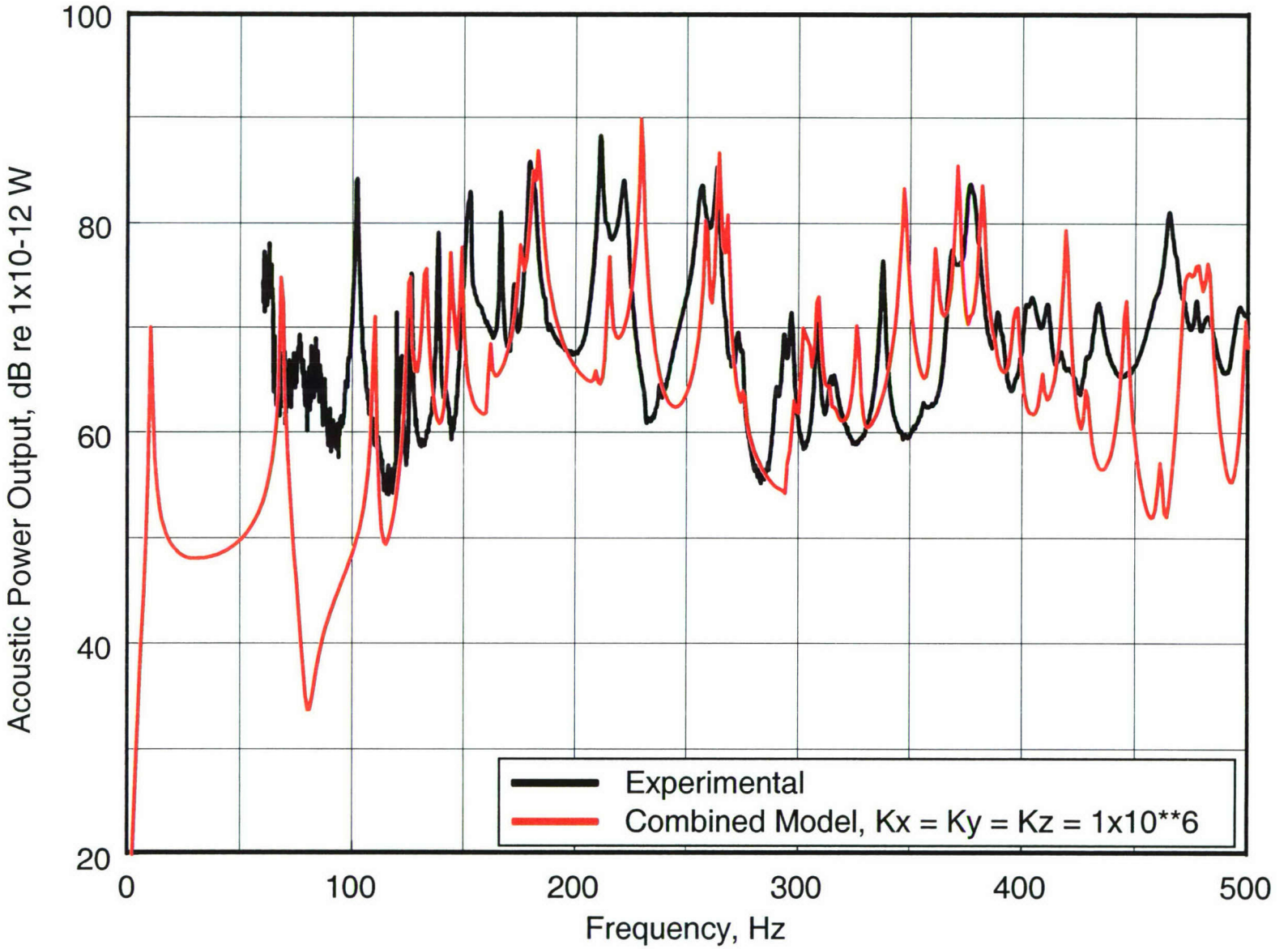

Figure 34. Experimental measurements and numerical predictions for the acoustic power output of the enclosure with the shelf clamped